TOPICAL REVIEW • FREE ARTICLE

Roadmap on solar water splitting: current status and future prospects

Sheng Chu[1,6], Wei Li[2], Yanfa Yan[3,6], Thomas Hamann[4,6], Ishiang Shih[1], Dunwei Wang[2,6] and Zetian Mi[1,5,6]

Published 28 September 2017 • © 2017 IOP Publishing Ltd
Nano Futures, Volume 1, Number 2

sheng.chu@mcgill.ca
yanfa.yan@utoledo.edu
hamann@chemistry.msu.edu
dwang@bc.edu
ztmi@umich.edu

[1] Department of Electrical and Computer Engineering, McGill University, 3480 University Street, Montreal, Quebec H3A 0E9, Canada

[2] Department of Chemistry, Boston College, Merkert Chemistry Center, 2609 Beacon Street, Chestnut Hill, MA 02467, United States of America

[3] Department of Physics and Astronomy & Wright Center for Photovoltaics Innovation and Commercialization, The University of Toledo, Toledo, OH 43606, United States of America

[4] Department of Chemistry, Michigan State University, 578 S Shaw Lane, East Lansing, MI 488241322, United States of America

[5] Department of Electrical Engineering and Computer Science, University of Michigan, Ann Arbor, 1301 Beal Avenue, Ann Arbor, MI 48109, United States of America [6] Authors to whom any correspondence should be addressed.

Thomas Hamann https://orcid.org/0000-0001-6917-7494

Received 26 July 2017
Accepted 25 August 2017
Accepted Manuscript online 25 August 2017
Published 28 September 2017

Method: Single-blind
Revisions: 2
Screened for originality? Yes

Sheng Chu et al 2017 Nano Futures 1 022001 https://doi.org/10.1088/2399-1984/aa88a1

Abstract

Artificial photosynthesis via solar water splitting provides a promising approach to storing solar energy in the form of hydrogen on a global scale. However, an efficient and costeffective solar hydrogen production system that can compete with traditional methods using fossil fuels is yet to be developed. A photoelectrochemical (PEC) tandem cell consisting of a p-type photocathode and an n-type photoanode, with the photovoltage provided by the two photoelectrodes, is an attractive route to achieve highly efficient unassisted water splitting at a low cost. In this article, we provide an overview of recent developments of semiconductor materials, including metal oxides, nitrides, chalcogenides, Si, III–V compounds and organics, either as photocathodes or photoanodes for water reduction and oxidation, respectively. In addition, recent efforts in constructing a PEC tandem system for unassisted water splitting are outlined. The importance of developing a single-photon photocathode and photoanode that can deliver high photocurrent in the low bias region for efficient PEC tandem system is highlighted. Finally, we discuss the future development of photoelectrode materials, and viable solutions to realize highly efficient PEC water splitting device for practical applications.

1. Introduction

Sunlight is the most abundant renewable energy resource and considered to be the ultimate solution to address the global energy problem: 'The Terawatt Challenge.' However, the

vision of solar energy providing a substantial fraction of global energy infrastructure is still far from being realized. The major challenge is to develop an efficient and cost-effective approach for storing solar energy that can be used on demand on a global scale. Solar water splitting provides a scalable route to store solar energy in the form of energy-dense hydrogen fuel [1], which can be directly used in a fuel cell with water as the only emission or as a reactant for well-established industrial processes, such as ammonia synthesis (Haber−Bosch reaction) or methanol production (CO_2/CO hydrogenation reaction). For solar water splitting systems, there are three major categories: photochemical (PC) system, photoelectrochemical (PEC) cell, and photovoltaic-electrolysis (PV-E), as shown in figure 1.

PV-E is a straightforward strategy of connecting two existing developed technologies: photovoltaic (PV) cell and water electrolyzer. Although PV-E have been demonstrated with high solar-to-hydrogen (STH) conversion efficiencies over 10% [2–9], this route is still too costly to compete with traditional methods using fossil fuels (e.g. steam reforming of natural gas) [10]. Considering the technological maturity of PV-E, further improvement in the efficiency has been limited. Therefore, the development of alternative and cost-effective routes to produce solar hydrogen is of particular interest. PC approach is a simple and lowcost process for potential solar hydrogen production, but this route is inefficient with a STH efficiency typically at least one order of magnitude lower (<1%), and produces a potentially explosive mixture of H_2 and O_2, which requires an external high-cost process to separate them to avoid back reactions [11]. In this context, PEC system, which lies intermediate between PV-E and PC, offers a high STH efficiency at an affordable cost [12–14]. The PEC approach integrates the light absorption and electrochemical process of PV-E process into a single and monolithic unit via a direct semiconductor–electrolyte interface to reduce the cost, while having a distinct advantage over PC system in that the H_2 and O_2 evolution halfreactions occur on two different electrodes and are separated physically. Recent technoeconomic analysses have shown that PEC water splitting can achieve substantially lower overall system cost compared to PV-E approach, and can become economically competitive with existing fossil-fuel derived hydrogen if the efficiency and lifetime are substantially improved to >10% and >5 years, respectively [14–16].

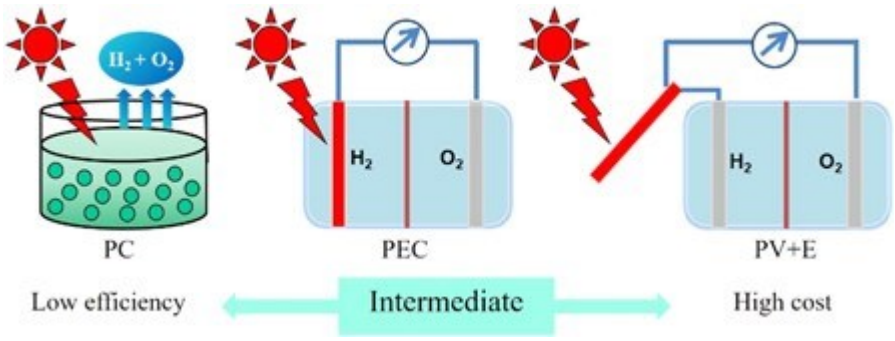

Figure 1. Schematic of three types of solar water splitting system: PC system, PEC cell, and PV-E. PC and PV-E have the respective limitations of low efficiency and high cost, while PEC lies intermediate for achieving high efficiency at an affordable cost.

A simple PEC configuration includes one semiconductor photoelectrode (as either photocathode or photoanode) and one standard metallic (dark) electrode (e.g. Pt). Ideally, the semiconductor should have an appropriate bandgap and band structure to encompass a large portion of solar spectrum while providing sufficient potentials to accomplish the overall water splitting reaction, as well as excellent charge transport properties and longterm stability during the operation. Despite the fact that many materials have been explored over nearly half a century, there is currently no single material that can fulfill all of the key criterion. Since overall water splitting consists of two half-reactions, i.e., water oxidation and proton reduction, it is natural to use a 2-photon dual-electrode system, which is analogous to the Z-scheme in natural photosynthesis. Compared to the PV-biased PEC tandem device, a simple tandem system consisting of spatially separated p-type photocathode and n-type photoanode is preferred in terms of cost, complexity and stability [17–19]. The energy band diagram for this type of device in a 'wireless' configuration is shown in figure 2. There are two designs of the device, depending on whether the wider bandgap material is a photoanode or a photocathode. In both designs, the longer wavelength photons that are not absorbed by the top large bandgap absorber are transmitted and harvested by the bottom low bandgap absorber. Owing to the band bending, the photogenerated electrons in p-type photocathodes and holes in n-type photoanodes migrate toward the semiconductor–liquid interface to reduce and oxidize water, respectively, while holes in the photocathode and electrons in the photoanode recombine at the ohmic contact that connects both photoelectrodes. As each material is responsible for the relevant half reaction of water splitting, the tandem system allows the use of smaller bandgap material

and relaxes the stringent requirement of band edge positions to straddle the water redox potentials. Therefore, the PEC tandem device can achieve potentially higher efficiency than the single absorber system, with large solar spectral coverage and a wide window of suitable materials to choose from (figure 3) [20–23]. Recently, various theoretical modeling studies have evaluated the achievable STH efficiency of this tandem system by considering different bandgap combinations [24–31]. Despite the varying results of the different models which include accounting for variable losses (e.g. kinetic overpotentials, solution ohmic resistance and parasitic light loss), it is generally accepted that such a tandem device can yield an STH efficiency over 25%. To achieve STH efficiency >20%, the optimal top and bottom semiconductor absorbers in a tandem device are with bandgaps of approximately 1.6–1.8 eV and 0.9–1.2 eV, respectively. The maximum STH efficiency of ~27% was predicted using the 1.7/1.1 eV bandgap combination [31], which can cover the major portion of solar spectrum with a current matching condition between the two photoelectrodes, as shown in figure 4.

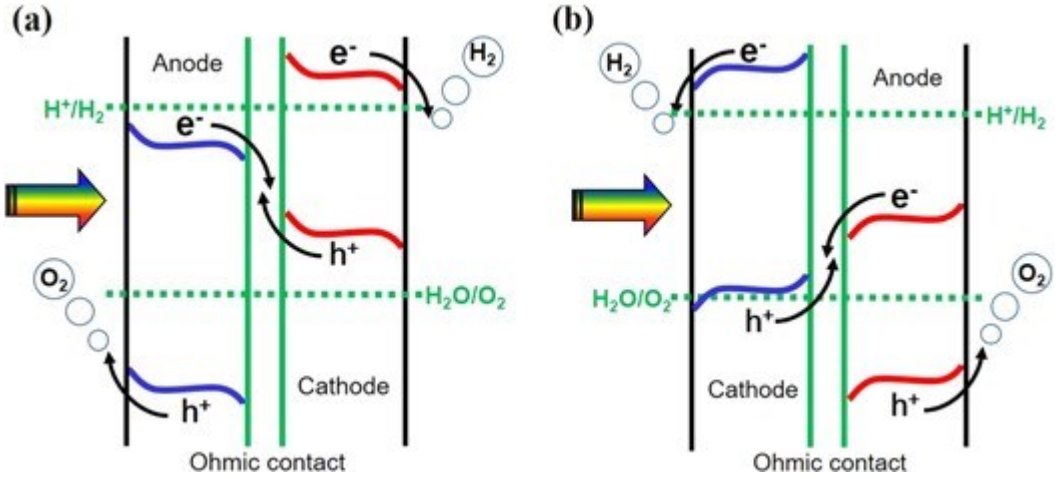

Figure 2. Schematic of tandem PEC water splitting device with (a) a large bandgap photoanode and a small bandgap photocathode and (b) a large bandgap photocathode and a small bandgap photoanode.

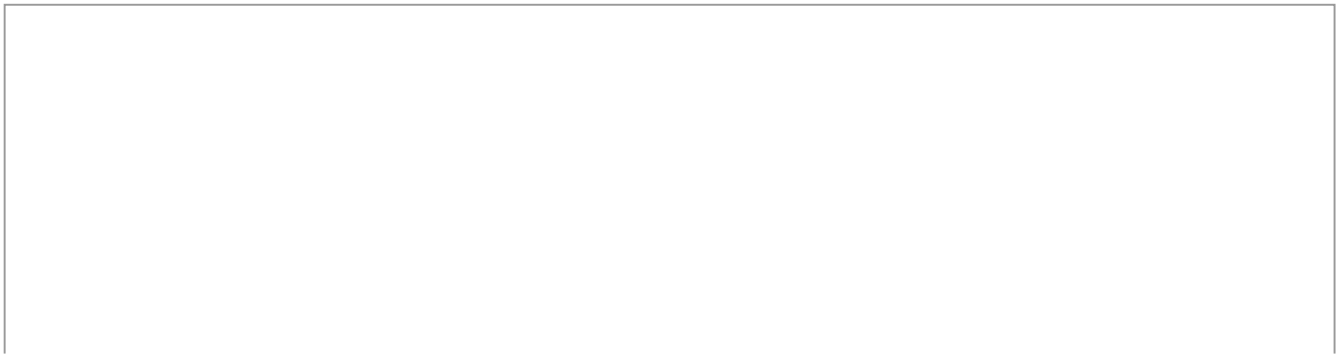

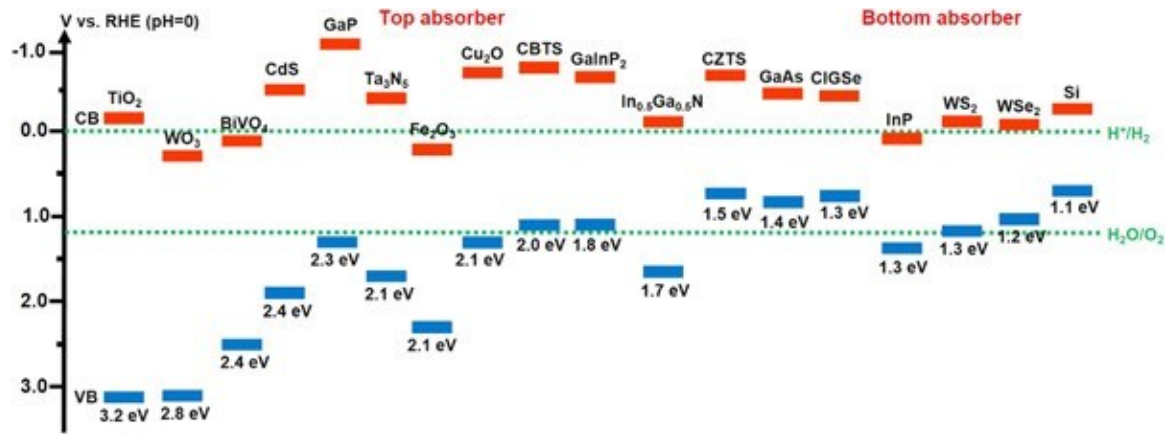

Figure 3. Bandgaps and band edge positions of various semiconductors with respect to the redox potentials of water splitting (pH = 0). The wide and narrow bandgap materials can be used as top and bottom absorbers, respectively. RHE: reversible hydrogen electrode. CB: conduction band. VB: valence band. CBTS: Cu_2BaSnS_4. CZTS: Cu_2ZnSnS_2. CIGSe: $Cu(InGa)Se_2$.

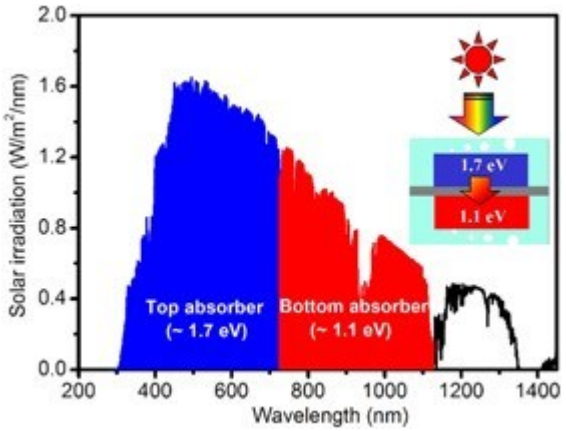

Figure 4. Solar spectrum (AM 1.5 G) coverage by a tandem PEC water splitting device with optimum bandgaps of ~1.7 and ~1.1 eV. Inset is the illustration of the tandem device.

In this review article, we focus on the recent progress in the development of promising semiconductor materials, including metal oxides, nitrides, chalcogenides, Si, III–V compounds and organics, either as photocathodes or photoanodes to construct potentially efficient p–n PEC tandem system for unassisted water splitting. First, the fundamental

principles of solar water splitting at a semiconductor/liquid junction (SCLJ), including different cell configurations and merits of parameters are introduced. Then great emphasis is focused on the design and development of efficient p- and n-type semiconductor materials as photocathode and photoanode for water reduction and oxidation, respectively. In addition, efforts to form a PEC tandem device by combining p-type photocathode and ntype photoanode for unassisted water splitting are summarized in terms of their STH efficiency and stability. Finally, conclusions and future prospects of solar water splitting for achieving a practical artificial photosynthesis device are presented.

2. Basic principles of solar water splitting

2.1. Semiconductor photoelectrochemistry

Semiconductor photoelectrochemistry deserves special attention because the system features a highly unique interface—the SCLJ. For a typical system where the Fermi level of the semiconductor is not at the same level as the electrochemical potential of the electrolyte prior to contact (figure 5(a)), the formation of the junction suggests that one or both of the energy levels should move to reach equilibrium. As the charge density of the electrolyte is typically several orders of magnitude higher than that of the semiconductor, hence semiconductor Fermi level is moved to align with the electrochemical potential of the electrolyte. While the same description would be true for a metal/liquid junction, the semiconductor is unique because it can form a relatively wide depletion region (up to μm's, depending on the dielectric constant, the carrier density, and the energy difference) [32, 33]. As is seen in figure 5(b), a SCLJ with a bent band is effectively a Schottky-type diode that can

separate photogenerated charges. This junction is the fundamental reason why semiconductor photoelectrochemistry is interesting.

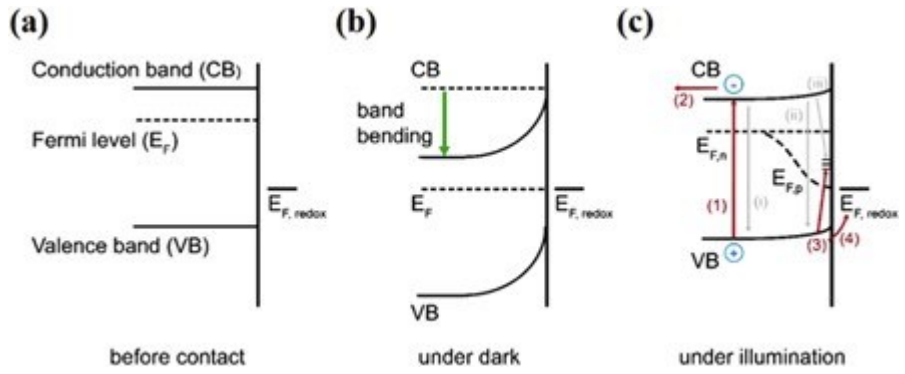

Figure 5. Schematic of the band diagrams under different conditions. (a) Prior to contact between the semiconductor and the electrolyte. (b) Upon contact under equilibrium conditions without light. (c) Quasi-equilibrium with illumination. The various processes are labeled as follows. (1) Charge excitation by light; (2) electron extraction through back contact; (3) hole transfer to surface states; (4) hole transfer to the electrolyte; (i) bulk recombination; (ii) surface recombination; (iii) electron trap by surface states.

On a practical level, semiconductor photoelectrochemistry also represents a useful tool to understand the detailed processes that govern the operation of a photocatalytic system. Consider solar water splitting as an example. In order to achieve high efficiencies, we desire to have a system that is efficient in all three major processes: absorbing light, separating charges, and driving hydrogen and oxygen evolution reactions. Careful studies of the SCLJ can help us understand which parts of the system are responsible if a system fails to deliver the expected performance. For instance, the performance of a photoanode as shown in figure 6 may be limited by any of the following processes. First, the recombination of electrons and holes in the bulk is too severe. Second, the direct recombination of electrons and holes in the conduction and valence bands, respectively, near the surface is too fast. More explicitly, charge distribution near the surface differs from the bulk. When majority charge carriers deplete from semiconductor to liquid, the minority charge concentration increases in this near-surface region forming an inversion layer, opening up additional recombination channels [34]. Third, surface mediated electron and hole recombination contributes significantly to the annihilation of photogenerated charge carriers. Fourth, charge carrier transfer from the semiconductor to the electrolyte is too sluggish to compete

with charge recombination processes as outlined above. Being able to accurately describe the various processes is critical to the understanding and, ultimately, solving the various issues for high-efficiency solar water splitting. Below, we will briefly present the equations that are useful to describe the SCLJ in a semiconductor PEC system.

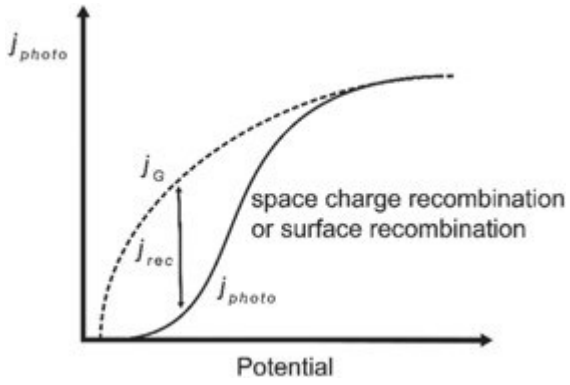

Figure 6. Idealized photocurrent–voltage relationship of a photoelectrode (broken line) and the one for a realistic system (solid line).

For the ease of discussions, we choose to use a photoanode system as shown in figure 5 as a prototypical platform to lay out the details. Upon contact, the SCLJ results in the formation of a space charge region (depletion region of electrons), whose width (W_{sc}) depends on the difference between the Fermi level of the semiconductor in vacuum and the electrochemical potential of the electrolyte ($\Delta\phi_{sc}$), the relative permittivity (ε) and the doping density (N_d):

$$W_{sc} = \left(\frac{2\Delta\varnothing_{sc}\varepsilon\varepsilon_0}{qN_d}\right)^{1/2}. \quad (1)$$

The capacitance of the space charge region can be derived from the variation of the space charge (Q_{sc}) with the potential drop ($\Delta\phi_{sc}$), $C_{sc} = dQ_{sc}/d\Delta\phi_{sc}$, as described by the Mott–Schottky equation:

$$\frac{1}{C_{sc}^2} = \frac{2}{qN_d\varepsilon\varepsilon_0}\left(\Delta\varnothing_{sc} - \frac{k_BT}{q}\right). \quad (2)$$

Because the electrical field generated within the space charge region varies linearly from distance $x = W_{sc}$ to the surface ($x = 0$), the variation of electrical potential will be proportional to x^2 and can be represented as band bending (figure 5(b)). The degree of band bending is governed by the Fermi level difference between the semiconductor and the redox pair. This is analogous to a Schottky junction formed between a semiconductor and a high work function metal [35]. Under reverse bias conditions (positive potentials), the Schottky barrier is increased, which makes it more difficult for electrons to transfer from the semiconductor to the electrolyte. For an anode system, such charge transfer would be considered back electron transfer and should be minimized. Meanwhile, the enhanced band bending under reverse bias makes it easy for holes to transport to the surface for driving oxidation reactions. Conversely, under forward bias (more negative potential applied on semiconductor), the band bending will be reduced and it becomes easier for electron transport from conduction band for oxidizing redox species (a reduction reaction). Similar to a Schottky diode of an n-type semiconductor, however, holes are minority carriers, meaning that the current under reverse bias is limited. As such, we expect a photoanode to exhibit low reverse bias current. That is, negligible oxidation reactions would take place on a photoanode without illumination.

Upon illumination ($h\nu > E_g$), electron–hole pairs are generated within the semiconductor as a result of electrons excitation from the valance band to the conduction band (process 1 in figure 5(c)). At thermal equilibrium, the generation of electron–hole pairs from photon excitation is balanced by the recombination on a timescale $>10^{-9}$ s. Because these photogenerated charge carriers can equilibrate with the lattice vibration (phonons) on a timescale $<10^{-12}$ s, the populations can be described by Fermi–Dirac statistics [36]. A quasiFermi level can then be derived by simply interpreting the steady-state carrier concentration of holes as representing a quasi-equilibrium situation ($E_{F,p}$ in figure 5(c)). Similarly, a quasiFermi level of electrons is also obtained ($E_{F,n}$ in figure 5(c)). But since the electron concentration is expected to be similar to the equilibrium value, $E_{F,n}$ is typically close to that under equilibrium. From a thermodynamics perspective, the driving force for water oxidation on a photoanode originates from the free energy difference between electron and hole quasi-Fermi levels. The physical model of band bending near surface is still valid under such a circumstance. The magnitude of the quasi Fermi levels splitting determines the maximum photovoltage (V_{ph}) one photoanode can provide. Under the likely assumption that one can probe the $E_{F,n}$ through back contact under equilibrium conditions (e.g., through the measurement of the open circuit voltage, V_{oc}), the difference between the

E_F (under dark, figure 5(b)) and the $E_{F,n}$ (under illumination, figure 5(c)) represents the V_{ph} [37–40].

The recombination of photogenerated electron–hole pairs can take place either in bulk (process i in figure 5(c)) or near surface (processes ii and iii in figure 5(c)), which may involve processes such as Shockley–Read–Hall recombination (through levels associated with defects or impurities), radiation (band to band) recombination or Auger recombination [41]. The recombination in bulk follows a pseudo first order rate law due to the excess of majority carriers (electrons in n-type semiconductor), and is characterized by the minority carrier lifetime τ_{min}. This value ranges from nanoseconds in many compound semiconductors to milliseconds in ultrapure silicon [42]. Since the electrical field in bulk is limited, the minority carriers (holes in n-type semiconductor) generated in this region can only diffuse a certain distance before they are recombined, trapped or transferred to the electrolyte to drive oxidation reaction. This is one important bulk property of a semiconductor and characterized as minority carrier diffusion length L_{min}, which is determined by the diffusion coefficient D_{min}, the mobility of minority carriers μ_{min} and τ_{min}:

$$L_{\min} = \sqrt{D_{\min}\tau_{\min}} = \sqrt{\frac{k_B T}{q}\mu_{\min}\tau_{\min}}. \quad (3)$$

Ideally, a photoanode should have long L_{min}, comparable or greater than the characteristic thickness of the material, so that most photogenerated holes could diffuse to the surface to drive the desired oxidation reactions. By assuming hole–electron recombination in the space charge region is negligible, and that the recombination on the surface is minimum due to rapid interfacial holes transfer, we can calculate the hole flux J_h to the surface, and the incident photon to current conversion efficiency (IPCE) or external quantum efficiency (EQE), as follows,

$$J_{\mathrm{h}} = I_0\left(1 - \frac{\exp(-\alpha W_{\mathrm{SC}})}{1+\alpha L_{\min}}\right), \quad (4)$$

$$\mathrm{IPCE} = \frac{J_{\mathrm{h}}}{\mathrm{I}_0} = 1 - \frac{\exp(-\alpha W_{\mathrm{SC}})}{1+\alpha L_{\min}}, \quad (5)$$

where α is the absorption coefficient at a given wavelength. Of course, as an oversimplified description for an idealized situation, the Gartner equation would be inadequate to describe actual systems. It nonetheless defines the upper limit of the achievable quantum efficiencies based on the measurable photophysical constants of a material. The current voltage characteristics as predicted by the Gärtner equation is shown in figure 6. The current–voltage relationship for a realistic system is different primarily due to the loss of photogenerated holes. Specifically, the onset-potential (where the photocurrent starts) will be shifted toward the more positive direction (as depicted in figure 6). In addition,

recombination in the space charge region (process ii in figure 5(c)) can proceed through defects close to mid-band gap. The analytical expressions with these considerations were previously discussed by Reichman and El Guibaly et al [43–46]. Surface recombination (process iii in figure 5(c)) is yet another important factor to be considered. The situation is particularly important when surface hole concentrations are high due to reasons such as slow interfacial hole transfer. Surface states can also arise from crystal defects, surface dangling bonds and/or chemisorbed species. Further, the photogenerated holes trapped by surface states can be annihilated through recombination with electrons. It is important to note that the definition of surface states used here is rather broad. They may refer to electronic states within the band gap caused by a number of reasons, including surface chemisorbed species as a result of chemical reactions.

In a way, the Gartner equation and the Reichman correction consider the photophysical properties of the semiconductor, both in the bulk and near/on the surface, and predict the rate at which photogenerated charges that can potentially drive the chemical reactions in the electrolyte. The charges that are actually transferred to the electrolyte may be calculated by the charge transfer efficiency. Assuming the likely scenario that surface processes are first order relative to charge concentrations, we have,

$$\mathrm{TE} = k_{\mathrm{tran}}/(k_{\mathrm{tran}} + k_{\mathrm{rec}}), \tag{6}$$

where TE is the transfer efficiency, k_{tran} is the forward charge transfer rate constant, and k_{rec} is the charge recombination rate constant. The measured photocurrent densities can then be calculated as:

$$J_{\mathrm{meas}} = J_{\mathrm{h}} \times \mathrm{TE}. \tag{7}$$

2.2. PEC cell configurations

In the introduction, we discussed three types of solar water splitting systems: PC, PEC, and PV-E. Here, we will focus on different PEC cell configurations, which can be constructed either from a single p-type semiconductor as photocathode (or n-type semiconductor as photoanode), or two semiconductors connected separately (or in series).

For a single semiconductor PEC cell where only a half-reaction occurs on the working electrode, a counter electrode is required for the other half-reaction to complete the electrical circuit. Often, a reference electrode is connected to the working electrode to characterize external applied voltage. If necessary, to avoid product crossover, two compartments or ion exchange membrane will be present to separate the working and counter electrode. This three-electrode configuration is depicted in figure 7(a). To overcome

the thermodynamic barrier of water splitting and the potential loss caused by recombination processes, the working electrode should have a band gap of at least 1.6 eV [22]. However, if the band gap is too wide, the visible light absorption efficiency will be low. Other potential loss mechanisms include back contact and overpotential induced by poor catalytic activity. To address this issue, the semiconductor material should be deposited on highly conductive substrate to form a good Ohmic contact, which allows rapid injection of majority carriers from working electrode to counter electrode. Additionally, HER or OER catalyst is required to facilitate surface kinetics accordingly.

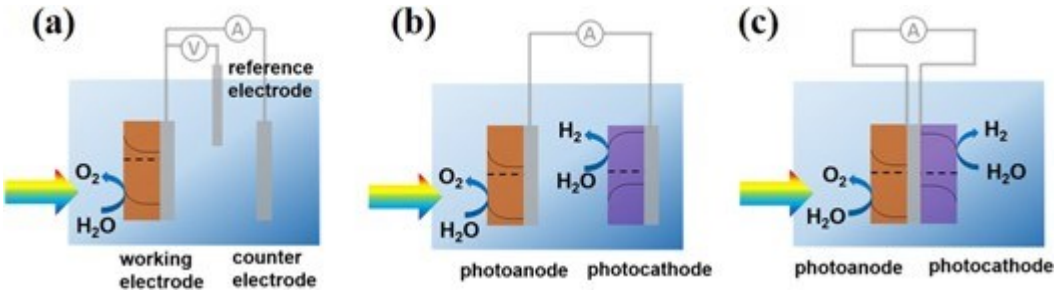

Figure 7. Schematic of basic components of PEC cell for (a) a single band gap photoanode with a metal cathode. (b) A photoanode and a photocathode connected separately in a tandem configuration. (c) A photoanode and a photocathode electrically connected in series in a back-to-back configuration.

As seen here, it is challenging for a single photoelectrode to achieve sufficient photovoltage for solar water splitting. The combination of dual semiconductors will be more advantageous. A second photoelectrode can replace the counter electrode where the other half-reaction occurs, and compensate the insufficient photovoltage (shown in figure 7(b)). The illumination should be directed from the larger band gap photoelectrode (transparent substrate) to the smaller band photoelectrode for better light utilization. Alternatively, these two semiconductors can form a wireless back-to-back Ohmic contact, sharing one transparent conductive substrate [21]. By doing this, potential loss in electrolyte and pH gradient between two photoelectrodes can be reduced [47]. Similarly, the illumination should pass through a larger band gap material to a smaller one. This tandem cell configuration is shown in figures 2 and 7(c), promising a relatively cost-effective device structure.

2.3. Calculation of efficiencies

To evaluate performance of solar water splitting, it is well acknowledged to compare onset potentials, and photocurrent density (normalized to projected surface area of photoelectrode) at 1.23 V versus RHE for photoanode and 0 V versus RHE for photocathode. Normalized metrics based on energy input, product conversion, etc. are of equal significance. Since the value-added product of water splitting is hydrogen, STH efficiency is the most critical figure of merit for measuring the performance and efficiency of solar water splitting on practical device level. It is defined as the ratio of output chemical/electric energy to input solar energy via the following equation:

$$\eta_{\mathrm{STH}} = \left[\frac{\phi_{\mathrm{H_2}}(\mathrm{mol\ s^{-1}\ m^{-2}}) \times G^{0}_{\mathrm{f,H_2}}(\mathrm{kJ\ mol^{-1}})}{P_{\mathrm{light}}(\mathrm{W\ m^{-2}})}\right]_{\mathrm{AM\ 1.5G}}, \tag{8}$$

where Φ_{H2} is the hydrogen gas production rate, G^{0}_{f,H^2} is the Gibbs free energy of hydrogen gas (237 kJ mol^{-1} at 25 °C) and P_{light} is the total solar irradiation input. The light source should match solar spectrum of air mass 1.5 global (AM 1.5 G). As mentioned, a STH efficiency over 20% is desired for large-scale application in the future, and a maximum 27% STH efficiency has been predicted for a 1.7 eV/1.1 eV tandem cell configuration with optimal light absorption (figure 4) [31]. Alternatively, output chemical energy can be substituted by electric energy that multiplies short-circuit current density j_{sc} and the redox potential of interest (1.23 V for water oxidation). Since 100% of the current may not contribute to the redox reaction, Faradaic efficiency must be considered in the equation. Faradaic efficiency (η_F) describes the efficiency of passing charges contributing to desired electrochemical reaction, which is defined as the ratio of the measured product quantity and the theoretical value derived by passing charges.

$$\eta_{\mathrm{STH}} = \left[\frac{j_{\mathrm{sc}}(\mathrm{mA\ cm^{-2}}) \times 1.23\ \mathrm{V} \times \eta_{\mathrm{F}}}{P_{\mathrm{light}}(\mathrm{mW\ m^{-2}})}\right]_{\mathrm{AM\ 1.5G}} \tag{9}$$

In general, the value of j_{sc} can be replaced by the externally measured current density at zero applied potential under steady-state conditions, which is analogous to short circuit conditions.

The STH efficiency is of particular interest to evaluate the performance of unassisted overall solar water splitting system. Extensively, to evaluate the performance of a single photoelectrode independently, where extra applied potential is often required from a second photoelectrode or external power supply, another concept of conversion efficiency can be introduced. At a certain j_{sc} and η_F, applied bias photon to current conversion efficiency (ABPE) can be written as follows:

$$\mathrm{ABPE} = \left[\frac{j_{SC}(\mathrm{mA\ cm^{-2}}) \times (1.23V - V_{app}) \times \eta_F}{P_{light}(\mathrm{mW\ m^{-2}})}\right]_{\mathrm{AM\ 1.5G}}, \quad (10)$$

where V_{app} is the applied potential between photoelectrode and counter electrode.
In addition to the conversion efficiencies characterized by the entire solar spectrum on a device level, it is important to understand the efficiency of electrons/holes converted from photons at individual wavelengths of light on a single photoelectrode material level. To serve this purpose, IPCE or EQE mentioned above can be written in an alternative format as follows:

$$\mathrm{IPCE}(\lambda) = \mathrm{EQE}(\lambda) = \frac{\text{electron flux (mol s}^{-1})}{\text{photon flux (mol s}^{-1})} = \frac{|j_{ph}(\mathrm{mA\ cm^{-2}}| \times hc(\mathrm{V\ m})}{P_\lambda(\mathrm{mW\ cm^{-2}}) \times \lambda(\mathrm{nm})} \quad (11)$$

in which λ is the single wavelength light source, P_λ is the power of irradiation, h is Plank's constant, c is the speed of light, and j_{ph} is the photocurrent density. To acquire IPCE, a monochromator (single wavelength light source) and a three-electrode configuration are essential, that j_{ph} at the identical applied potential with individual wavelengths of light can be obtained accurately. Generally, the onset wavelength is closely related to the bandgap of semiconductor. In addition, by integrating the IPCE values with the standard AM 1.5 G solar spectrum, the total photocurrent density under solar illumination can be estimated as,

$$J_{\mathrm{AM\ 1.5}} = \int (\mathrm{IPCE}_\lambda \times \phi_\lambda \times e)\mathrm{d}\lambda \quad (12)$$

where e is the elementary electron (C) and ϕ_λ is photon flux of irradiation (m^2 s).

3. Advances in the development of PEC water splitting

3.1. Photocathode materials

3.1.1. Metal oxide

Because of its earth abundance, nontoxicity, high mobility, good and natural p-type electric conductivity and close to optimum direct bandgap of 2.1 eV, cuprous oxide, Cu_2O, is considered a promising candidate for photocathodes for PEC water splitting, with a theoretical maximum photocurrent of 14.5 mA cm^{-2} and a STH efficiency of about 18% [48–50]. Though Cu_2O has favorable band energy positions for water splitting, its application as an efficient and durable photocathode for water splitting has been inhibited by its poor photostability in aqueous electrolytes and low photocatalytic efficiency caused by fast recombination of minority carriers (electrons). Extensive research efforts have been made to improve the photostability by employing protective layers, such as ZnO, TiO_2, and SnO_2 [50–53], to reduce recombination of carriers by coupling with other semiconductors

such as CuO, Ga_2O_3, WO_3, and Al-doped ZnO (AZO) [50, 53–56], to form p–n heterojunctions and enhance charge transfer by applying co-catalysts, such as Pt, RuO_2, and MoS_2 [50, 57–59]. In 2011, Grätzel and co-workers showed that a Cu_2O photocathode could be significantly stabilized with protective coatings of AZO and TiO_2 deposited by atomic layer deposition (ALD) [50]. Recently, using a Cu_2O nanowire photocathode with AZO/TiO_2 protection layers and RuO_x catalyst, Grätzel and co-workers reported photocurrent density as high as 10 mA cm^{-2} at −0.3 V versus RHE [60]. The photocurrent density was maintained for over 55 h. The results demonstrate the promise of Cu_2O as a photocathode for PEC water splitting.

In terms of photovoltage, Cu_2O was reported with a relatively negative onset potential (typically 0.4–0.6 V versus RHE), which need to be combined with photoanodes that can provide large photovoltage to form PEC tandem device for unassisted water splitting. Recently, by introducing a Ga_2O_3 buffer layer between the Cu_2O and TiO_2 protective layer, an extremely positive onset potential of 1.02 V versus RHE was produced [61], which represents an important step to pair with a narrow bandgap photoanode such as Si.

Besides binary Cu_2O, there are many efforts to develop Cu-based ternary oxides as photocathodes, such as $CuFeO_2$ and $CuBi_2O_4$. $CuFeO_2$ is an attractive material due to its earth abundant composition and suitable bandgap of 1.5 eV. Read et al first reported $CuFeO_2$ photocathode, prepared by a facile electrochemical process, produced a highly positive onset potential of 0.98 V versus RHE but a low photocurrent density of 0.3 mA cm^{-2} at 0.4 V versus RHE [62]. Later, Jang et al demonstrated a much-enhanced photocurrent of 2.4 mA cm^{-2} at 0.4 V versus RHE by using strategies including post-annealing and electrocatalyst modification to improve the poor charge transport properties and surface reaction kinetics, respectively [63]. Notably, $CuFeO_2$ has been demonstrated with stable operation for 40 h in the presence of O_2-sacrificial electron scavenger [64]. $CuBi_2O_4$ is another promising photocathode material, which features a suitable bandgap of 1.6–1.8 eV as the ideal top light absorber in the PEC tandem device. $CuBi_2O_4$ was first identified as a potential photocathode material by Arai et al in 2007 through a combinatorial screening study [65], which was later experimentally confirmed by Hahn et al [66]. Recently, a photocurrent of 1.2 mA cm^{-2} at 0.1 V versus RHE was reported by using Pt as the co-catalyst [67]. It is worth mentioning that $CuBi_2O_4$ can produce an extremely positive onset potential >1.0 V versus RHE due to its positive flat-band potential above 1.3 V [68, 69], which makes it a very promising photocathode material as the top cell in the PEC tandem device if the charge carrier properties and catalytic activity can be further improved.

3.1.2. III–V group materials

III–V materials hold record efficiencies for both single-junction and multiple-junction solar cells [70]. Owing to their tunable optoelectronic properties, high light absorption coefficient, and exceptional charge-transport properties, III–V semiconductors, including GaP, InP, and their alloy compounds such as GaInP, are reported with extremely high efficiency as photocathode materials [71]. However, III–V semiconductors suffer severely from rapid photocorrosion in the electrolyte, which requires additional protection layers to prevent the direct contact from the electrolyte. Lee et al demonstrated the stable operation of p-InP nanopillars photocathode coated with a thin layer of TiO_2 (3–5 nm) grown by ALD, in conjunction with Ru co-catalyst [72]. It was reported that the photocathode had a high conversion efficiency of ~14% under simulated AM 1.5 G illumination. In addition to the role as the surface protection layer, Lin et al found the thin TiO_2 layer could reduce the surface recombination and enhance the photovoltage of planar-based InP photocathodes [73]. After the deposition of TiO_2, there was an anodic shift of 200 mV, which produced a high onset potential over 800 mV. Recently, Gao et al developed a periodic array of InP nanopillars photocathode with a buried p–n^+ junction [74]. Owing to the rational control of interface energetics and minimization of light reflectance, the photocathode produced an unprecedented onset potential of 850 mV (figure 8(a)), which was close to the open-circuit potential of InP homojunction solar cells (0.939 V) [70]. Moreover, the device yielded a high photocurrent over 25 mA cm^{-2} at a positive potential as high as 0.6 V versus RHE and a benchmarking power conversion efficiency of 15.8% for single junction photocathodes, which promises high efficiency unassisted water splitting when paired with a highperformance photoanode. With the protection of a thin layer of TiO_2 (4 nm), the photocathode exhibited stability for at least 6 h, in contrast with the fast decay of sample without TiO_2 protection (figure 8(b)).

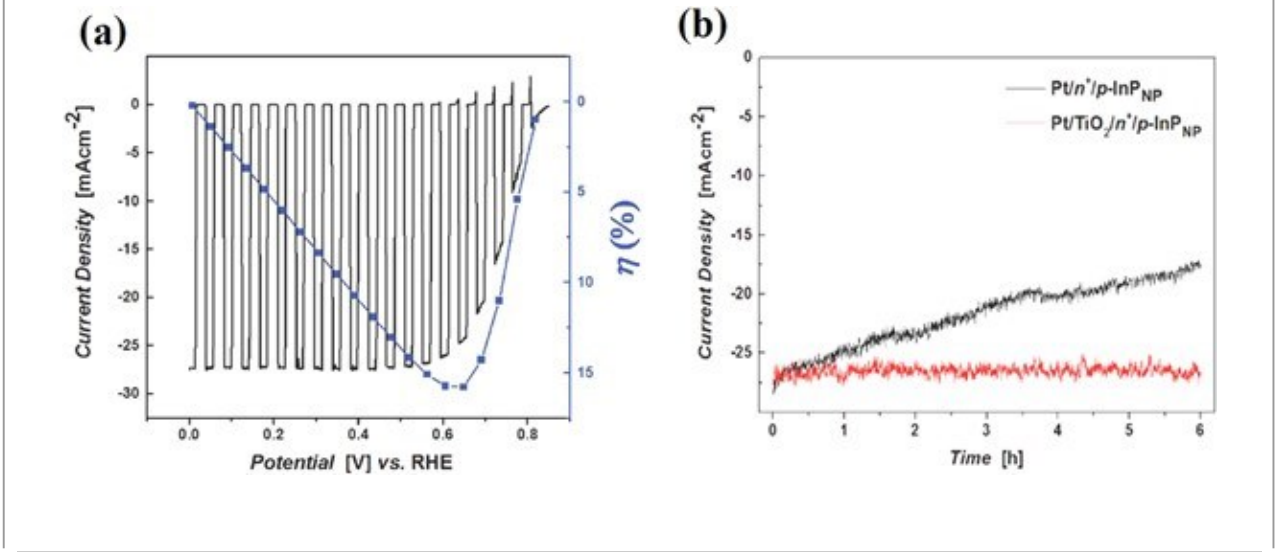

Figure 8. (a) Photocurrent density–potential (J–V) curve (black solid line) and power conversion efficiency (η, blue squares) of Pt/n^+/p-InP photocathode in 1 M $HClO_4$ under chopped AM 1.5 G illumination. (b) Stability test of Pt/n+/p-InP (black line) and Pt/TiO_2/n+/p-InP (red line) at 0 V versus RHE in 1 M $HClO_4$ under continuous AM 1.5 G illumination. [74] John Wiley & Sons.

Recently, III-nitride semiconductors, e.g. GaN and InGaN, have emerged as a new generation of materials for solar hydrogen production [75–81]. In contrast to the poor PEC stability of conventional III–V compounds, wherein the chemical bonds are mostly covalent, III-nitrides exhibit extreme stability in aqueous solution due to their ionic bonding character [82, 83]. In addition, they possess similar, or even better optical, electrical, and structural properties than conventional III–V compounds. For example, InGaN is the only known semiconductor material whose bandgap can be tuned while straddling the water redox potentials over a wide range of solar spectrum (UV, visible, and even near-infrared light) [84]. Also, spontaneous polarization can be obtained in III-nitrides with N-terminated surfaces, which could enhance the charge transport and separation for efficient overall solar water splitting and protect the surface against oxidation and photocorrosion [85]. Moreover, compared to the high cost of conventional III–V compounds, it is worth mentioning that III-nitride materials, widely used in the semiconductor industry including solid-state lighting and power electronics, are much more attractive for cost-effective and scalable production.

In 2005, Fuji et al demonstrated the great potential of p-GaN as photocathode for H_2 evolution [86]. Afterwards, Aryal et al reported higher photocurrent density on p-InGaN

compared to p-GaN, and its excellent stability for a prolonged period of 24 h in HBr solution without any protection layer [87]. Recently, Fan et al developed an integrated InGaN/Si photocathode for efficient and stable H_2 evolution [88]. In conjunction with Pt co-catalyst, the monolithic device exhibited a high photon-to-current efficiency of 8.7% with unity faradic efficiency for H_2 generation. Moreover, without any additional protection layer, it showed stable operation without degradation for at least 3 h, promising high potential to construct a PEC tandem water splitting system.

3.1.3. Cu-based chalcogenides

Cu-based chalcogenides such as chalcopyrites and kesterites have demonstrated their potential for fabricating efficient thin-film PV solar cells [70], owing to their excellent properties such as high optical absorption, suitable bandgap, and defect tolerance [89–94]. Since PV and PEC water splitting share the same fundamental working principle on photon absorption and charge carrier generation and separation, Cu-based chalcopyrites and kesterites are naturally considered promising candidates for efficient PEC water splitting. Owing to their suitable conduction band edge for hydrogen evolution, Cu chalcopyrites and kesterites have been extensively studied in the last decade as photocathodes for PEC water reduction.

The Cu chalcopyrites have a general compositional formula of I-III-VI_2 (I = Cu, II = In, Ga; VI = S, Se), for example CuInSe (CISe), $CuInS_2$ (CIS), $CuGaSe_2$ (CGSe), and $CuGaS_2$ (CGS) [95]. The chalcopyrites can be considered derivatives of the II–VI compounds such as ZnS by replacing the two group II atoms by one group I atom and one group III atom. The chalcopyrite structure resembles the zinc-blend structure, in which the cations are tetrahedrally coordinated by four group VI anions. The kesterites can be further considered derivatives from the chalcopyrites by replacing two group III atoms by one group II and one group IV atoms, giving a general compositional formula of I_2-II-IV-VI_4 (II = Zn; IV = Sn), i.e., Cu_2ZnSnS_2 (CZTS) and $Cu_2ZnSnSe_2$ (CZTSSe) [96]. The kesterite structure resembles the chalcopyrite. The atomic structures of CIS chalcopyrite and CZTS kesterite are shown in figures 9(a) and (b), respectively. Cu_2BaSnS_4 (CBTS) exhibits a trigonal crystal structure with space group $P3_1$ (see figure 9(c)) [97], in which each Cu and Sn is tetrahedrally surrounded by sulfur ions. Two Cu-derived and one Sn-derived tetrahedrons share a corner and thus each sulfur atom is three-fold coordinated with two Cu and one Sn. Ba atoms are located at the interstitial sites in the tetrahedral framework, forming rows along the [100] and [010] directions. The orthorhombic $Cu_2BaSnSe_4$ (CBTSe) has very similar structure as the trigonal CBTS, but it crystallizes in space group Ama2 [97], shown in figure 9(d).

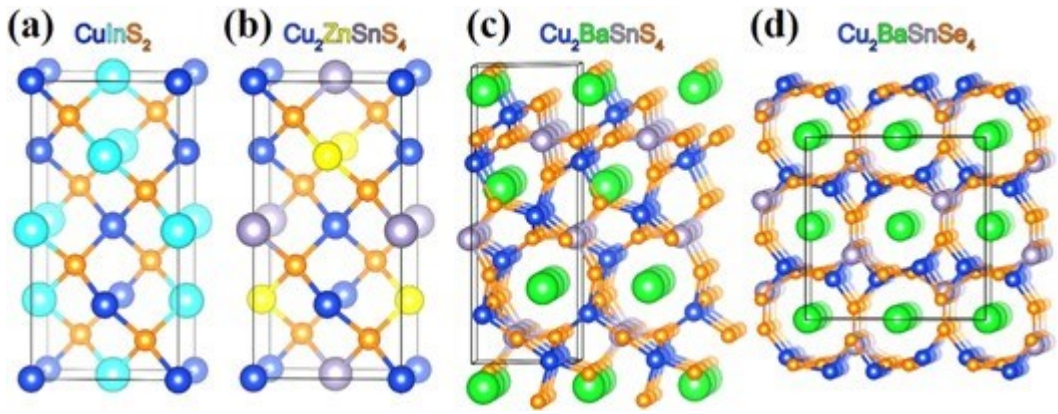

Figure 9. Crystal structures of (a) chalcopyrite CIS; (b) kesterite CZTS, (c) trigonal CBTS, and (d) orthorhombic CBTSe.

Cu chalcopyrites and kesterites have direct bandgaps, while trigonal CBTS and orthorhombic CBTSe have nearly direct bandgaps, i.e., the difference between the direct and indirect bandgap values is very small [98, 99]. The bandgaps of the four quaternary Cu chalcopyrites are 1.00 eV (CISe), 1.54 eV (CIS), 1.68 (CGSe), and 2.43 eV (CGSe). The alloyed chalcopyrites of Cu(In, Ga)(S, $Se)_2$ can cover the bandgap range from 1.0–2.4 eV, by tuning the In/(In + Ga) and S/(S + Se) atomic ratios, as shown in figure 10 [93]. The bandgaps of the two quarternary Cu kesterites are 1.0 eV (CZTSe) and 1.5 eV (CZTS). The alloyed kesterites of CZT(S, Se) can cover the bandgap range from 1.0–1.5 eV, by tuning the S/(S + Se) ratio. The bandgap value is about 1.95 eV for trigonal CBTS and 1.64 for orthorhombic CBTSe. The alloyed system of CBT(S, Se) shows a bowing effect with a phase transition at the composition of around $Cu_2BaSnSe_3S$. The smallest bandgap was found to be 1.52–1.55 eV [100].

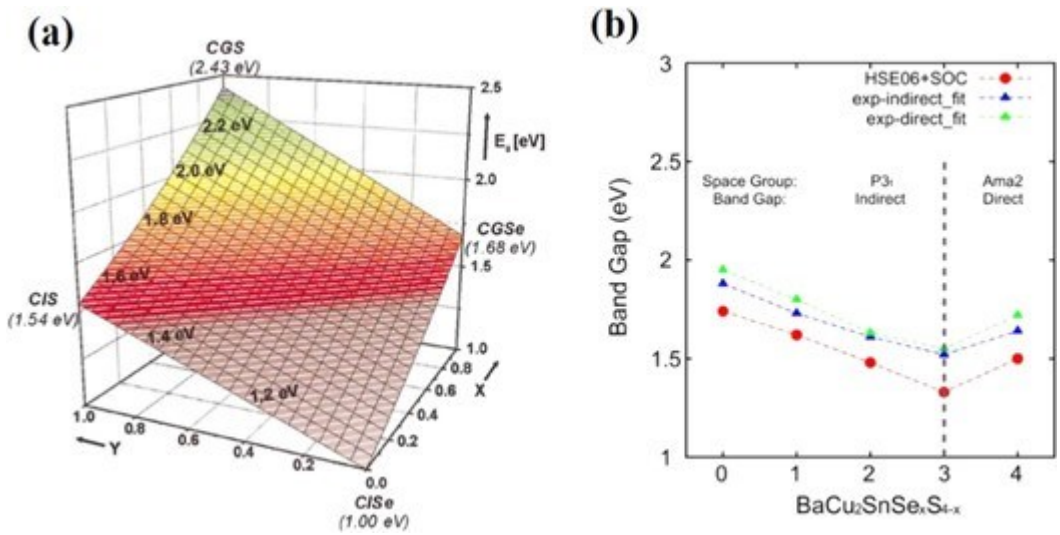

Figure 10. (a) Optical band gap energies of the complete $Cu(In_{1-x}Ga_x)(S_ySe_{1-y})_2$ chalcopyrite system for 0 <= x <= 1 and 0 <= y <= 1. The colors correspond to the light sensation of the human eye. Reprinted with permission from [93]. Copyright 2004, AIP Publishing LLC. (b) Evolution of band gap values, obtained using diffuse reflectance data on powder (bulk) samples, with increasing Se content in the $BaCu_2SnSe_xS_{4-x}$ ($0 \le x \le 4$) solid solution (green and blue lines marked with triangles for direct and indirect band gap fits, respectively) and calculated fundamental gaps (HSE06 functional with spin–orbit coupling) using the experimental lattice parameters with internal atomic positions optimized using the HSE06 functional (red line, circles). Reprinted with permission from [100]. Copyright 2016 American Chemical Society.

For PEC water splitting applications, non-radiative recombination is highly undesirable since the recombination will reduce the photovoltage of PEC device, resulting in a reduced conversion efficiency. The non-radiative recombination is mostly caused by defects with energy levels deep in the bandgap of the absorber. It has been shown that the high efficiencies of CIGSe thin-film solar cells are primarily attributed to the defect tolerance properties of CIGSe absorbers [92]. Theoretical studies have shown that the antibonding coupling between fully occupied Cu 3d and Se 4p orbitals raises the valence band maximum of CIGSe, which consequently makes Cu vacancies (V_{Cu}) very shallow acceptors [94]. Furthermore, the antibonding nature energetically favors the formation of Cu vacancies, making them the dominant defects in CIGSe [91]. However, for chalcopyrites with larger bandgaps such as CGSe, the defect tolerance is decreased due to the formation of Cu and Ga antisite defects [92]. CZTSe and CZTS also exhibits antibonding coupling

between fully occupied Cu 3d and Se 4p/S 3p orbitals and the Cu vacancies are also shallow acceptors [90]. However, recently, density functional theory calculations have shown that trigonal CBTS and orthorhombic CBTSe have larger bandgaps suitable for PEC water splitting and exhibit defect tolerance properties better than wide-bandgap Cu chalcopyrites such as CGSe and CGS and kesterites CZTS and CZTSe. Due to the very different electronic properties between the cations, the CBTS and CBTSe do not easily form the cation–cation defects [98, 99]. Therefore, CBTS and CBTSe and their alloys are promising candidates for the applications of efficient PEC water splitting.

Recently, Cu chalcopyrite and kesterite photocathodes have been extensively investigated [101–112]. Some noticeable results reported in literature are summarized in table 1. The highest photocurrent reported for CGSe photocathode without n-type partners and catalysts is 10.6 mA cm^{-2} at 0 V versus RHE [101]. The CZTS photocathodes produced much lower photocurrents without n-type partners and catalysts. The highest photocurrent was reported only 1.3 mA cm^{-2} at 0 V versus RHE [110]. Using CdS as a n-type partner and Pt as catalyst, CIS, CIGS, and CZTS photocathodes showed much improved photocurrents. For example, the photocathode of Pt/Mo/Ti/CIGSe has shown a photocurrent of 30 mA cm^{-2} at 0 V versus RHE and a power conversion efficiency of 8.5% [106]. A Pt/In_2O_3/CdS/CZTS photocathode showed a photocurrent of 9.3 mA cm^{-2} at 0 V versus RHE and a power conversion efficiency of 1.63% [112]. Very recently, the PEC performance of CBTS and CBTSSe photocathodes have also been reported [113–117]. So far the TiO_2/ZnO/CdS/CBTS photocathode showed the highest photocurrent, about 7.2 mA cm^{-2} at 0 V versus RHE under Xe lamp irradiation (100 mW cm^{-2}), reported by Ge et al [114].

Table 1. Representative results of Cu-based chalcogenide photocathodes under AM 1.5 G simulated one sun illumination.

Photocathode	Electrolyte	Photocurrent at 0 V versus RHE	Power conversion efficiency	Year [reference]
CGSe	0.5 M H_2SO_4	10.6 mA cm^{-2}	—	2008 [101]
Pt/CdS/CGSe	0.1 M Na_2SO_4 pH 9	7.5 mA cm^{-2}	0.83% (0.2 V versus RHE)	2013 [102]

Photocathode	Electrolyte	Photocurrent at 0 V versus RHE	Power conversion efficiency	Year [reference]
Pt/In_2S_3/CIS	0.1 M Na_2SO_4 pH 9	15 mA cm^{-2}	1.97% (0.28 V versus RHE)	2014 [103]
Pt/TiO_2/CdS/CIS	0.1 M NaH_2PO_4 pH 10	13 mA cm^{-2}	1.82% (0.25 V versus RHE)	2014 [104]
Pt/ZnO/CdS/CIGS	0.5 M Na_2SO_4 pH 9	32.5 mA cm^{-2}	—	2015 [105]
Pt/Mo/Ti/CIGSe	0.5 M H_2SO_4 + 0.25 M Na_2HPO_4 + 0.25 M NaH_2PO_4 pH 6.8	30 mA cm^{-2}	8.5% (0.38 V versus RHE)	2015 [106]
Pt/CdS/CIGS	0.2 M NaH_2PO_4 pH 10	6.0 mA cm^{-2}	0.66% (0.21 V versus RHE)	2015 [107]
Pt/TiO_2/CdS/CIS(Bi)	0.5 M Na_2SO_4/0.25 M NaH_2PO_4/0.25 M NaH_2PO_4 pH 6.1	8.0 mA cm^{-2}	—	2016 [108]
Pt/TiO_2/CdS/CZTS	0.1 M Na_2SO_4 pH 9.5	9.0 mA cm^{-2}	1.2% (0.22 V versus RHE)	2010 [109]
CZTS	0.3 M Na_2SO_4 pH 9.5	1.3 mA cm^{-2}	—	2015 [110]
Pt/CdS/CZTS	0.2 M NaH_2PO_4 pH 10	1.2 mA cm^{-2}	—	2016 [111]
Pt/In_2S_3/CdS/CZTS	0.2 M NaH_2PO_4/NaH_2PO_4 pH 6.5	9.3 mA cm^{-2}	1.63% (0.31 V versus RHE)	2015 [112]

3.1.4. Si

Si, the most widely used semiconductor in PV industry, is suited for the bottom light absorber in the PEC tandem system, given its narrow bandgap of ~1.1 eV. Its appropriate conduction band edge for hydrogen evolution, which in principle can produce a relatively large photovoltage, renders it an attractive candidate for a photocathode [118]. Despite the high-performance for solar hydrogen evolution, bare Si photocathode undergoes rapid

etching or oxidization when in direct contact with electrolyte. To overcome the issue of instability, a conformal-coated protective layer, including metallic layer and metal oxide layer, have been employed to passivate the surface states of Si to improve their stability. Despite the parasitic light absorption/reflection issue, metals can be employed as protection layers without compromising charge carrier transport owing to their excellent conductive properties. Maier et al demonstrated a 60 d long-term stable operation in 1 M HCl (aq) using Pt-coated p-Si photocathode [119]. Transparent metal oxides (e.g. TiO_2) have recently been widely investigated as protective layers due to their high intrinsic chemical stability and optical transmittance in the visible light region. Owing to the alignment of TiO_2 conduction band with respect to the Si conduction band and hydrogen evolution potential, TiO_2 facilitate the electron transfer from Si to electrocatalyst surface with negligible resistance [120]. It was found that the TiO_2 protected p–n^+ Si photocathode could keep working for over 30 d of operation under red-light (38.6 mW cm^{-2}; $\lambda > 635$ nm) filtered, simulated sunlight (as the bottom cell in the PEC tandem device) [121].

Onset potential is an important parameter to evaluate the potential of a photoelectrode to construct a PEC tandem system. Crystalline p-Si yielded a low onset potential of at most 400 mV, even in conjunction with Pt co-catalyst [122]. By introducing a buried metallurgical n^+– p junction, the onset potential was increased up to 560 mV due to the larger band bending at the n^+/p interface relative to the p-Si/electrolyte interface [123]. Recently, by using ultrathin amorphous Si (a-Si) as the passivation layer, a high positive onset potential of 640 mV was observed on buried junction crystalline Si (c-Si) photocathode [124]. In addition, the a-Si/cSi heterojunction produced a STH conversion efficiency of 13.26%, which is the highest among the reported Si-based photocathodes. In terms of onset potential, the highest value of 930 mV was reported on a-Si based photocathode, which largely attributed to the enlarged bandgap of a-Si (~1.7 eV) and an optimized solid junction for charge carrier separation [125]. In conjunction with a TiO_2 protection layer and Pt co-catalyst, the a-Si photocathodes exhibited an impressive photocurrent of over 10 mA cm^{-2} at a positive potential as high as 0.6 V versus RHE under simulated one sun illumination (figure 11). In addition, the photocathode showed a high stability for at least 12 h of operation.

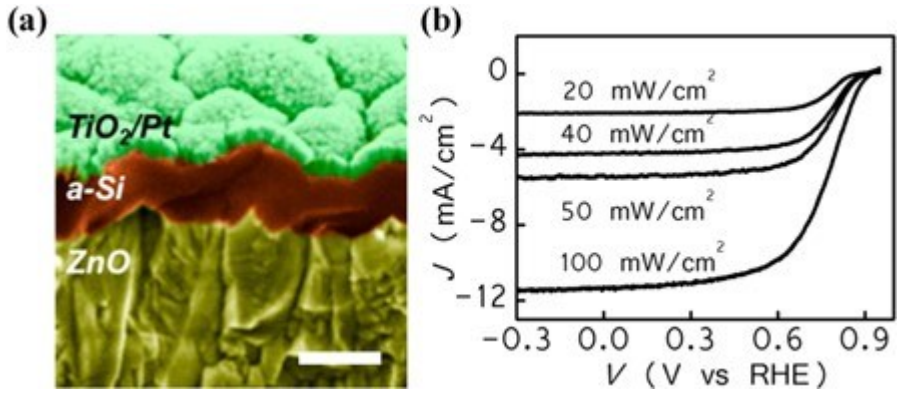

Figure 11. (a) Scanning electron microscope image shows the cross-section of an a-Si photocathode with Pt as catalyst. Scale bar is 400 nm. (b) J–V plots of a representative a-Si photocathode under different simulated solar illumination intensities in 0.5 M aqueous potassium hydrogen phthalate solution. Reprinted with permission from [125]. Copyright 2013 American Chemical Society.

3.1.5. Other emerging materials

Recently, semiconducting transition metal dichalcogenides (TMDs) such as WS_2, WSe_2, MoS_2 and $MoSe_2$ have emerged as very promising materials for solar hydrogen evolution owing to their distinct properties including suitable bandgap energy (1–2 eV), high light absorption coefficients (10^5–10^6 cm^{-1}) and chemical robustness without additional protection layer [126–128]. The layered crystal structure of TMDs can be exfoliated into mono- or few-layer two-dimensional (2D) sheets, with the bandgap to be finely tuned as the top/bottom light absorber according to the number of atomic layers. In 1983, Baglio et al reported Pt-coated p-WS_2 (1.3 eV) photocathode with a hydrogen evolution efficiency of 6%–7% and an open-circuit potential of ~800 mV in 6 M H_2SO_4 [129]. Recently, McKone et al reported p-WSe_2 (1.2 eV) as photocathode with a solar energy conversion efficiency over 7% and excellent stability with a Pt–Ru co-catalyst [130]. With controlled doping, surface engineering, and increased understanding of the role of edge states and defects, it is

envisaged that the performance of these 2D TMDs can be further improved in the foreseeable future.

In addition to the TMDs, semiconducting organic materials (e.g. conjugated polymers) have recently received increasing attention for solar hydrogen production due to their chemical versatility and facile low-cost solution processability [131–134]. Their electronic and optical structure can be rationally controlled at the molecular level towards suitable bandgap and energy levels to match well with the water redox potentials [135–138]. Although PV cells with power conversion efficiencies over 10% have been demonstrated [70, 139], solar energy conversion efficiencies over 1% for PEC water splitting have only been realized very recently
[140, 141]. For example, Rojas et al reported a relatively high photocurrent of 8 mA cm^{-2} at 0 V versus RHE with an onset potential of ~0.7 V versus RHE on a poly(3-hexylthiophene):phenyl-C 61-butyric acid methyl ester (P3HT:PCBM) bulk heterojunctionbased photocathode enclosed between a cuprous iodide hole-selective layer and a Ptdecorated nanostructured TiO_2 layer [141]. The photodegradation of the device was partially suppressed by the addition of a polyethyleneimine protective coating layer. It is noteworthy that the performance of organic photocathode is far from being optimized and further development can be expected by rational choice of the building block, hole/electron selective layer, protection layer and co-catalyst.

3.2. Photoanode materials

3.2.1. Metal oxides

Metal oxides are extensively studied as photoanode materials due to their high photostablity and low-cost preparation. Early studies were mainly focused on wide bandgap materials, such as TiO_2 (E_g = 3.0–3.2 eV) and $SrTiO_3$ (E_g = 3.2 eV), which features excellent stability and favorable band edge positions straddling the water redox potentials [142–145]. However, the large bandgaps limit the light absorption mainly in the ultraviolet region, which accounts for only ~4% of the solar spectrum. Although doping can extend the light absorption into the visible region, limited success has been achieved due to the accelerated charge recombination and reduced stability associated with doping. Recently, great attention has been paid to the intrinsically visible-light-responsive materials, such as Fe_2O_3 (E_g = 2.0–2.2 eV) and $BiVO_4$ (E_g = 2.4 eV) [146–149].

α-Fe_2O_3 (hematite) has been considered as a promising photoanode material owing to its near-ideal bandgap for visible light harvesting, excellent chemical stability against

photocorrosion, low cost and abundance [150–153]. However, there are several drawbacks, including: (1) short hole collection length (2–4 nm); (2) short carrier lifetime (<10 ps); (3) low absorption coefficient (on the order of 10^3 cm^{-1}); (4) poor surface water oxidation kinetics and (5) relatively low conduction band position (~0.4 V versus RHE at pH = 0) with respect to the water reduction potential. Several strategies including doping, nanostructuring and co-catalyst modification were applied to address the above-mentioned limitations. As most of the studies focused on a single specific aspect of these modifications, the overall performance remains relatively low. Recently, by considering the synergistic effects of Pt-doping to improve the electrical conducting property, single-crystalline 'wormlike' nanostructure to shorten hole diffusion distance towards electrolyte, and Co–Pi modification to enhance the oxygen evolution reaction, a high photocurrent of 4.32 mA cm^{-2} was reported at 1.23 V versus RHE [154]. Very recently, by using a unique nanosheet morphology with a Co–Pi co-catalyst, together with plasmonic Ag nanoparticles to enhance the light absorption and charge transfer, a record photocurrent of 4.68 mA cm^{-2} was achieved at 1.23 V versus RHE [155]. This photocurrent corresponds to ~37% of the maximum theoretical limit expected for 2.1 eV bandgap hematite, indicating there are still much room for further improvement. To construct a PEC tandem device with a photocathode, the highly positive turn-on potential (typically at 0.8–1 V versus RHE) of hematite is an important disadvantage [156]. Recently, Wang and coworkers developed a facile re-growth strategy, together with decorations of $NiFeO_x$ co-catalyst, a record onset potential of 0.45 V versus RHE was achieved [157], which approached the flat band potential of hematite (~0.4 V versus RHE).

Another metal oxide that has gained significant attention recently is $BiVO_4$ [158–163]. The most appealing property offered by $BiVO_4$ is the relatively negative band edge positions, permitting a photovoltage >1 V. While a similar photovoltage has also been obtained on TiO_2, $BiVO_4$ absorbs significantly more visible light than TiO_2 (absorption cut-off at λ = 510 nm versus 380 nm) [164]. And compared to hematite, hole diffusion length is less of a limitation for $BiVO_4$ (~100 nm) [165]. However, owing to the existence of electron and hole polarons, unmodified $BiVO_4$ was reported with a low charge carrier mobility of 0.04 cm^2 V^{-1} s^{-1} [166]. To increase the low charge carrier mobility, doping is an effective strategy to enhance the carrier concentration in $BiVO_4$. For example, Luo et al reported Mo doping as shallow energy levels can enhance the conductivity of $BiVO_4$ by 80 times compared with undoped $BiVO_4$, resulting in a much improved PEC performance in natural seawater [158]. Recently, by using a nanoporous structure consisting of small $BiVO_4$ nanoparticles of 76 nm, a high charge separation efficiency of 90% was obtained at 1.23 V

versus RHE, indicating the bulk recombination was minimized [167]. With the application of two water oxidation catalysts, FeOOH and NiOOH, the resulting photoanode featured an onset potential as low as 0.2 V versus RHE and a photocurrent of 2.73 mA cm^{-2} at 0.6 V versus RHE [167]. With additional Mo doping, Qiu et al prepared nanoporous $BiVO_4$/Fe(Ni)OOH on a cone-shaped nanostructured substrate, which showed a photocurrent of 5.82 mA cm^{-2} at 1.23 V versus RHE [168]. In addition, recently, Kuang et al demonstrated a nanoworm $BiVO_4$ with a photocurrent of 3.2 mA cm^{-2} at 0.6 V versus RHE and long-term stability up to 10 h [169].

For better charge separation, constructing heterojunction has been proven as an effective strategy for various photoelectrodes [170, 171]. A core–shell heterojunction of $BiVO_4$/WO_3 was reported by Pihosh et al with Co–Pi as a water oxidation co-catalyst. This configuration allowed for a photocurrent of 6.72 mA cm^{-2} at 1.23 V versus RHE [172]. A recent study by Kim et al combined $BiVO_4$ and Fe_2O_3 as hetero-type dual photoanode, which reported a record photocurrent density of 7 mA cm^{-2} at 1.23 V versus RHE (figure 12) [173].

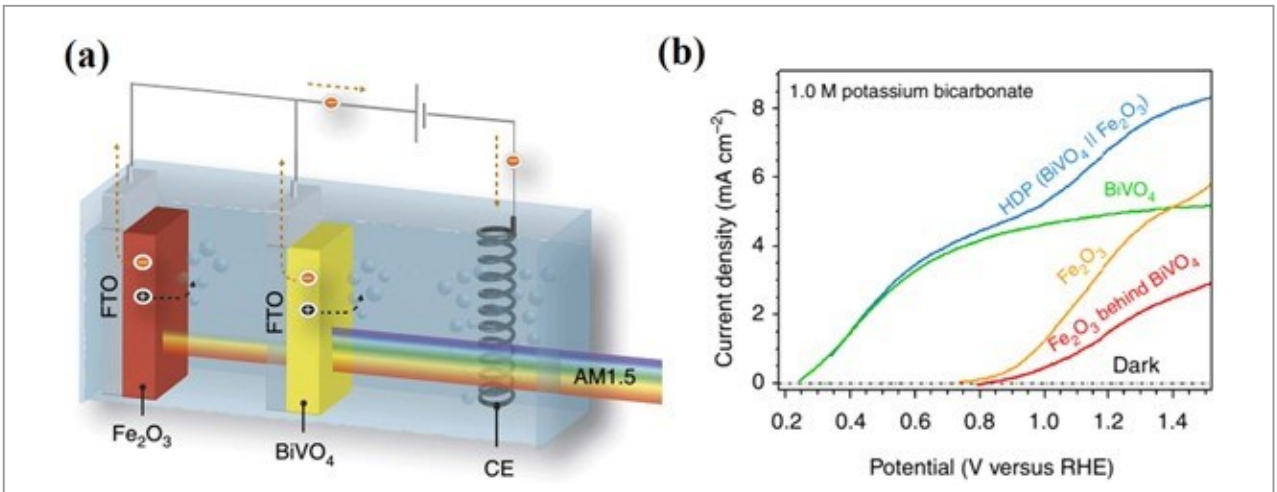

Figure 12. (a) Wavelength-selective solar light absorption by hetero-type dual photoanode consisted of $BiVO_4$ and Fe_2O_3. (b) J–V curves in 1.0 M KCi at pH = 9.2 under 1 sun illumination. Reproduced from [173]. CC BY 4.0.

Using $BiVO_4$ as a model case, some other ternary metal oxides with a smaller bandgap (E_g < 2.4 eV) have been investigated recently as promising photoanode materials to achieve higher theoretical STH efficiency, such as spinel ferrites (MFe_2O_4, M = Cu, Mg, Zn, etc) (E_g = 1.4–2.0 eV) [47, 174–178], $CuWO_4$ (E_g = ~2.3 eV) [179–184] and $FeVO_4$ (E_g = ~2.0 eV) [185–188]. Despite promising high theoretical photocurrent densities, however, the reported performance of these complex metal oxide photoanodes is still very low (typically

sub-mA cm^{-2} at 1.23 V versus RHE under simulated one sun illumination), which is largely limited by strong bulk recombination, unfavorable surface states that mediate water oxidation, and poor surface reaction kinetics. It is highly desirable to improve the performance by developing novel methods to synthesize/grow high quality complex metal oxides free from impurities/defects, and applying various strategies including nanostructuring, doping and co-catalyst modification to overcome the limitations.

3.2.2. Metal nitrides

Because of the lower electronegativity of N than O, the valance band consisting of N 2p orbitals is expected to be more negative than that of O 2p orbitals. Indeed, a number of nonoxide semiconductors have been shown to be more suitable for complete water splitting from a band edge position perspective [80, 189]. Among them, Ta_3N_5 is a prototypical material that deserves special attention. With a direct band gap of 2.1 eV, Ta_3N_5 promises overall water splitting at efficiency higher than 15% [190, 191]. It is noteworthy that neartheoretical limit photocurrent density has been reported (12.1 mA cm^{-2} at 1.23 V versus RHE) [191]. As is true for most non-oxide semiconductors, the most important challenge in using Ta_3N_5 for water splitting is its poor stability. Significant efforts have been attracted to address this challenge. For instance, Co_3O_4 [192], $Co(OH)_x$ [193, 194], Co–Pi [195] and NiFe-layered double hydroxide [196] have been shown to improve the stability of Ta_3N_5 to a certain extent. Notably, by using a GaN coating strategy to form a crystalline nitride-onnitride structure, a benchmarking 10 h stable operation with a high photocurrent density of 8 mA cm^{-2} was achieved, in conjunction with Co–Pi co-catalysts [197]. Nevertheless, the long-term stability of the Ta_3N_5-based photoanode remains to be improved for practical applications. Another challenge presented by Ta_3N_5 is the typical positive onset potential of ~0.6 V versus RHE, even though the band edge positions would predict a much more negative value. Some successes have been reported in this aspect. For example, a slight improvement of photovoltage (a 50 mV cathodic shift of onset potential) was achieved by Seo et al by using the combination of doping and surface treatment [198]. The origin of the two issues, poor stability and low photovoltage, however, has not been answered until very recently by Wang and coworkers [199]. It was found that the photo-oxidation of Ta_3N_5 is a self-limiting process rather than photocorrosion. A quantitative correlation between the degree of surface oxidation and the extent of surface Fermi level pinning was established, as shown in figure 13. As a result, the charge separation capabilities are dramatically undermined upon exposure to PEC water oxidation conditions.

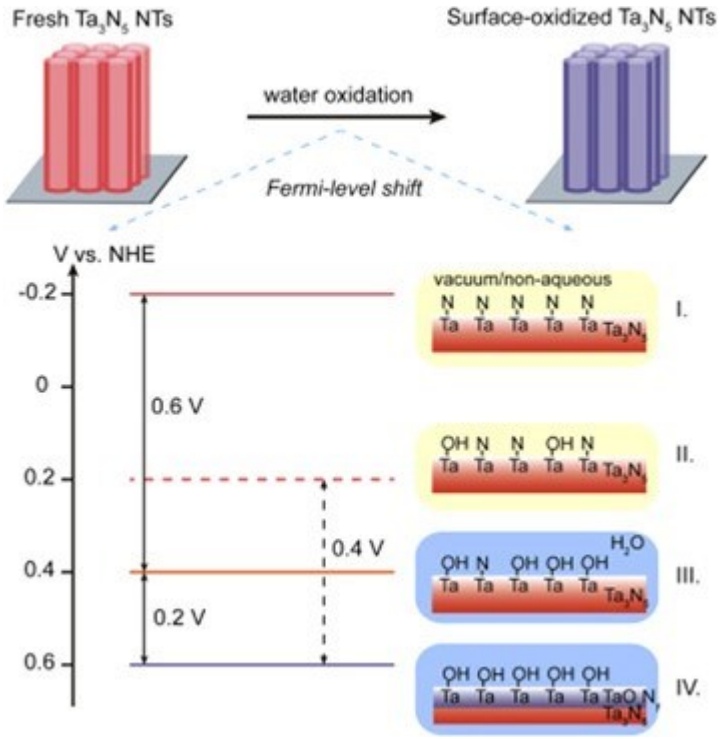

Figure 13. Schematic of how surface oxidation influences the electronic structures of Ta_3N_5. (I) Clean Ta_3N_5 features negative Fermi levels relative to normal hydrogen electrode (NHE). (II) Chemisorption of hydroxides positively shifts the Fermi level to 0.2 V versus NHE. (III) The Fermi level is further shifted toward the positive direction when Ta_3N_5 is immersed in H_2O. (IV) Photoelectrochemical reactions lead to non-reversible surface changes (the formation of $TaON_x$) that shift the Fermi level more positive. Reprinted from [199], Copyright 2016, with permission from Elsevier.

In addition to Ta_3N_5, complex metal (oxy)-nitrides such as $LaTiO_2N$ (E_g = 2.1 eV) [200–204], $BaTaO_2N$ (E_g = 1.9 eV) [205, 206] and $SrNbO_2N$ (E_g = 1.8 eV) [207], are promising photoanode materials as the top cell in a tandem device. For example, $BaTaO_2N$, modified with a Co co-catalyst, was reported to produce a photocurrent of 4.2 mA cm^{-2} at 1.2 V versus RHE with a stability for 6 h [206]. More importantly, the onset potential was observed below 0.2 V versus RHE, which is an advantage to integrate with a photocathode for realizing unassisted water splitting. To construct such a tandem device, it is important to use a transparent conductive substrate to transmit long wavelength light to the bottom cell. However, the high-performance nitride photoanode materials are generally synthesized under harsh conditions (>900 °C with NH_3) that are not compatible with typical transparent-conducting-oxide substrates, such as FTO (F-doped SnO_2), ITO (Sn-doped In_2O_3), and AZO (Al-doped ZnO). Recently, Hamann and co-workers reported the first example of Ta_3N_5 electrode directly synthesized on a transparent conductive substrate, Tadoped TiO_2 (TTO) [208]. This work represents a significant step towards constructing efficient tandem devices based on nitride photoanodes.

Recently, InGaN photoanodes have also been studied [209–217]. For example, Luo et al first demonstrated the high photostability of visible-light-responsive InGaN in aqueous HBr solution [210]. The IPCE was reported about 9% at 400–430 nm. In a subsequent study, by removing In-rich InGaN region using a simple electrochemical surface treatment, the IPCE was improved to 42% at 400 nm [212]. It was found that the In-rich InGaN phases played a major role as surface recombination centers of photogenerated charge carriers. As discussed previously, the energy bandgap of InGaN can be tuned across nearly the entire solar spectrum by varying the alloy compositions. However, due to the large lattice mismatch between InN and GaN (~11%), the synthesis of high-quality In-rich InGaN has remained difficult. Recently, Fan et al have shown that $In_{0.5}Ga_{0.5}N$ nanowires with nearly homogeneous indium distribution could be achieved by plasma-assisted molecular beam epitaxy [215]. Under AM 1.5 G one sun illumination, the InGaN nanowire photoanode exhibited a photocurrent density of 7.3 mA cm^{-2} at 1.2 V (versus NHE) in 1 M HBr. The IPCE is above 10% at 650 nm, which is not possible for most metal oxide photoanodes due to their wide bandgap. With the formation of InGaN/GaN core–shell structures, the photoanodes also exhibited a high level of stability, due to the surface passivation and protection by a thin GaN shell layer [216]. Recently, the atomic origin of the long-term stability and high efficiency of $[000\bar{1}]$ oriented III-nitride nanowire arrays for overall water splitting was investigated both experimentally and theoretically [85]. It was revealed that the

GaN nanowires exhibited N-termination, not only for their $(000\bar{1})$ top faces but also for their $(10\bar{1}0)$ side faces. Such N-terminated surfaces passivate the GaN nanowires against corrosion by air/aqueous electrolytes. More recently, Fan et al demonstrated an InGaN/Si double-band photoanode, with the nearly ideal bandgap configuration of 1.75 eV/1.13 eV for maximum STH conversion [217]. Under AM 1.5 G one sun illumination, the saturated photocurrent density reached 16.3 mA cm^{-2}, which is among the highest values reported for monolithically integrated tandem cells of such a nearly ideal energy bandgap configuration. The maximum power conversion efficiency of the InGaN nanowire/Si tandem photoanode was 8.3% at 0.5 V versus NHE in 1 M HBr solution.

3.2.3. Si and III–V group materials

Benefiting from the narrow bandgap and excellent charge carrier properties, Si and III–V group materials are also widely studied as photoanode materials. These materials, however, are less favorable to serve as photoanodes for water oxidation, compared to photocathodes for proton reduction. This is because the valence band edge positions of Si and most III–V semiconductors are too negative for water oxidation, which requires a high bias to proceed the reaction. For example, Si photoanode was reported with a typical onset potential of 0.9–1.1 V versus RHE [218–221], which is a challenge to pair with any high-performance photocathodes. In addition, Si and most III–V semiconductors can undergo photocorrosion under water oxidation conditions in aqueous electrolyte. Transparent conductive oxides have been shown to be very effective in passivating Si surface [222–227]. For example, the application of a highly uniform, 2 nm thick layer ALD TiO_2 coupled with Ir water oxidation catalysts, the stability of Si photoanode was extended to over 8 h under conditions with various pH [228]. The ultrathin TiO_2 layer allows the facile hole transport via tunneling mechanism. A novel study was presented by Kenney et al in which 2 nm Ni film on n-Si with native oxides was shown to serve as both a protection layer and a catalyst (figures 14(a) and (b)) [229]. In 1 M KOH, the resulting photoanode exhibited high PEC activity with an onset potential of 1.07 V versus RHE. The stability was examined in both 1 M KOH (up to 24 h) and LiBi–KBi electrolyte at intermediate pH (over 80 h). In a separate study, Hu et al demonstrated the utility of a novel 'leaky' amorphous TiO_2 layer (4–143 nm thick) deposited by ALD [230]. With the addition of Ni catalyst (which should be transformed to NiO_x upon oxidation and then to NiOOH upon PEC reactions), the Si photoanode enabled high photocurrent density (over 30 mA cm^{-2} with 100% Faradaic efficiency for O_2 production) over 100 h in 1 M KOH (figures 14(c) and (d)). Further study indicated that holes transported the defective TiO_2 layer though the mid-gap states and an ohmic contact was formed at the interface between TiO_2 and Si [231].

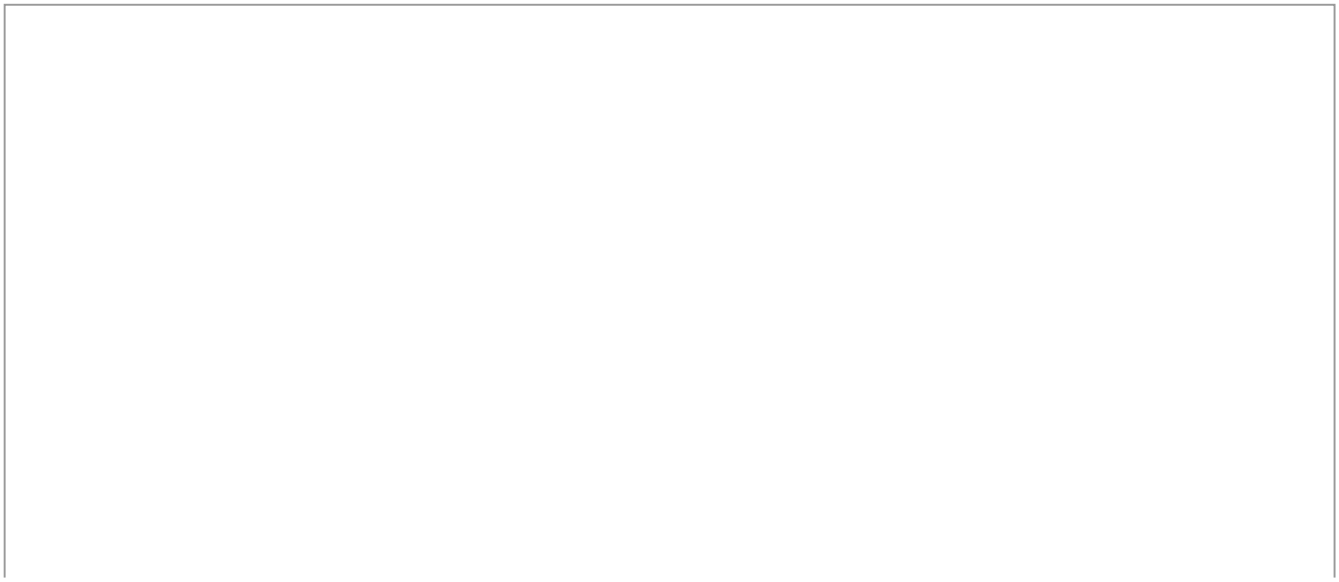

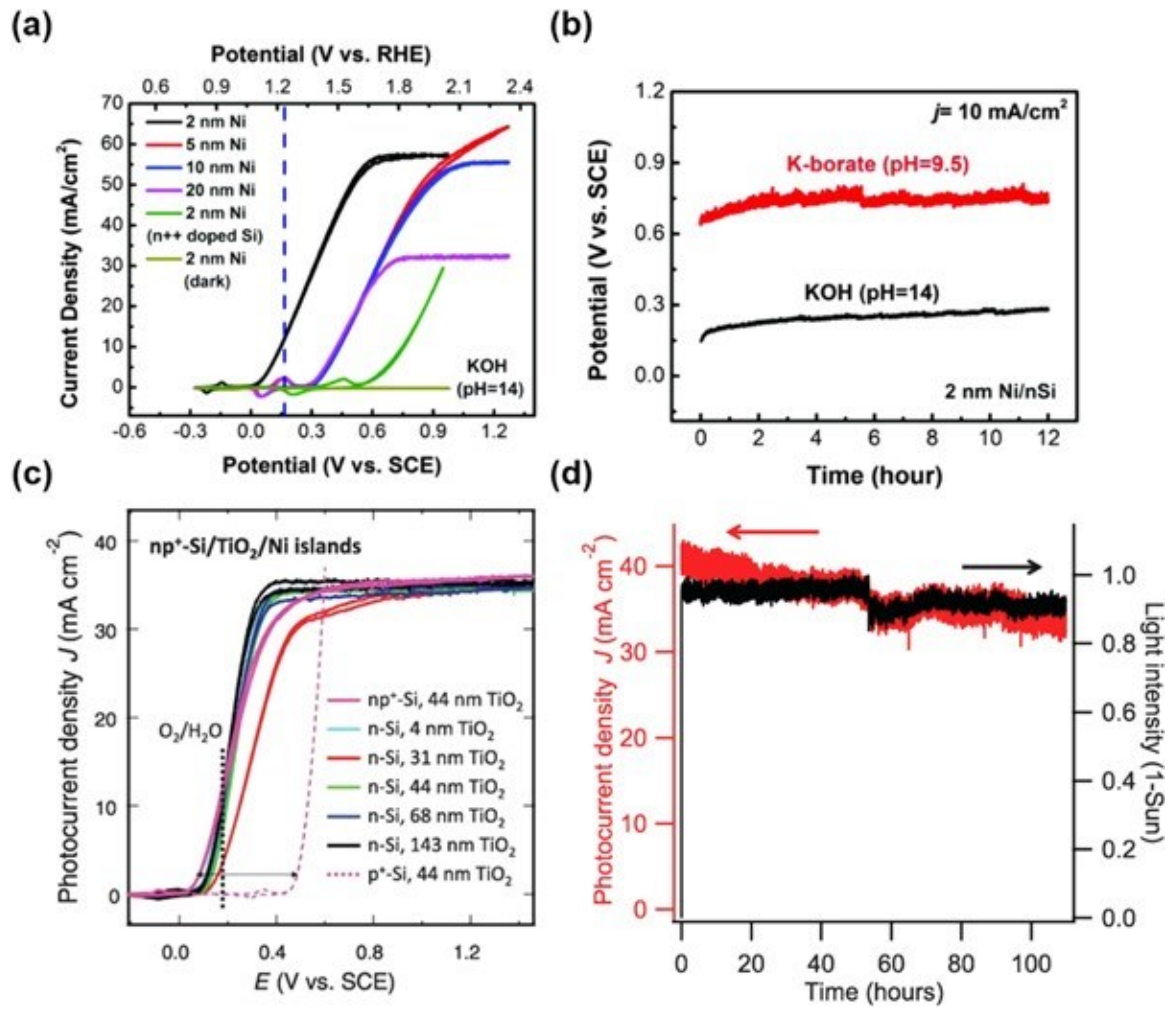

Figure 14. The stability of Si photoanode can be improved by thin Ni film (also as catalyst) or thick TiO_2 film (with Ni catalyst). (a) Cyclic voltammograms of various thickness Ni-coated n-Si anodes in 1 M KOH under illumination. From [229]. Reprinted with permission from AAAS. (b) Stability test fixed at constant current density of 10 mA cm^{-2}, of 2 nm Ni/n-Si anodes in 1 M KOH and 1 M K-borate under constant illumination. From [229]. Reprinted with permission from AAAS. (c) Cyclic voltammograms of various thickness TiO_2-coated n-Si anodes in 1 M KOH under illumination. From [230]. Reprinted with permission from AAAS. (b) Stability test fixed at 0.93 V versus SCE of 44 nm TiO_2/n-Si anodes in 1 M KOH under constant illumination. From [230]. Reprinted with permission from AAAS.

Similarly, transparent conductive oxides are commonly used as the protective layers for III–V photoanodes [230, 232, 233]. For example, 'leaky' TiO_2 layer are used to stabilize GaAs and GaP photoanodes for more than 100 h [230]. It is noteworthy that over 40 h stable operation with over 10% STH efficiency has been recently demonstrated on a

TiO_2protected buried GaAs/InGaP photoanode, in conjunction with Ni-based electrocatalysts [234].

3.2.4. Other emerging materials

Conjugated polymers emerged as a new type of photoanode material, although it is not favorable at the beginning because of the stability concerns. Recently, considerable efforts have been devoted to graphitic carbon nitride (g-C_3N_4)-based materials owing to its robust framework that established in photochemical water splitting since the pioneer work of Wang et al [235]. Initial studies by directly depositing the g-C_3N_4 powder on substrate resulted in a very small photocurrent (on the order of μA cm^{-2}), which was ascribed to the deleterious grain boundary effect and poor contact between g-C_3N_4 and substrates [236–238]. Very recently, using a vapor deposition approach to directly grow g-C_3N_4 film on substrates, an enhanced photocurrent of ~0.1 mA cm^{-2} at 1.23 V versus RHE was reported [239, 240]. In addition to g-C_3N_4, a ladder polymer, poly(benzimidazobenzophenanthroline), known as BBL, was also investigated as a photoanode [241]. A photocurrent up to 0.23 mA cm^{-2} was produced at 1.23 V versus RHE in the presence of sacrificial hole acceptor (SO_3^{2-}), while H_2O_2 or OH production instead of O_2 was observed for solar water oxidation. Although still at its early stage, further developments of polymer-based photoanodes are expected if the quality of film, poor conductivity and surface reaction kinetics are improved.

Recently, considerable efforts have also been devoted to investigating TMDs material such as MoS_2 as photoanode for water oxidation [242–244]. For example, MoS_2 nanosheet arrays photoanode was shown a high photocurrent up to 10 mA cm^{-2} at 1.23 V versus RHE and power conversion efficiency of 1.27% [244].

3.3. PEC tandem system

In the PEC tandem system, a p-type photocathode and an n-type photoanode with complementary bandgap absorption are integrated for the reduction and oxidation of water, respectively. Such a simple configuration offers potential advantages over PV-biased PEC tandem devices in terms of cost, complexity and stability. The intersection of the overlapped
J–V curves of photocathode and photoanode is the maximum operating current density (J_{OP}) for the overall water splitting system (no bias). As such, the overall water splitting activity largely depends upon the performance of individual photoelectrodes for each half reaction, particularly in the low bias region. Figure 15 shows a comparison of two hypothetical

photoanodes and photocathodes to construct a PEC tandem device. Although photoanode B and photocathode D give higher photocurrent densities at the high bias region, photoanode A and photocathode C are preferred electrodes to construct a more efficient tandem device as demonstrated by a higher J_{OP}. This clearly highlights the importance of achieving high photocurrent density at the low bias region for each photoelectrode in constructing efficient tandem device. Note that J_{OP} is the theoretical value estimated without considering Ohmic loss between the two photoelectrodes and parasitic optical loss caused by the top light absorber.

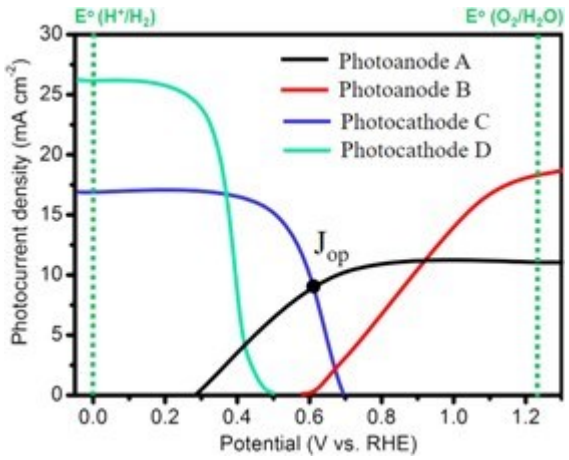

Figure 15. A comparison of J–V curves of four hypothetical photoelectrodes, including two photoanodes and two photocathodes, to construct a PEC tandem device. The combination of photoanode A and photocathode C gives the most efficient tandem device in terms of maximum operating current density (J_{OP}).

In the tandem device, there are two illumination modes: parallel illumination (Mode P) and tandem illumination (Mode T), as shown in figure 16. In Mode P, each photoelectrode is exposed to one beam of light, which allows the use of non-transparent substrate. While in Mode T, the solar energy is utilized more efficiently as the longer wavelength photons that are transmitted by the top absorber are absorbed by the bottom absorber. In this review, we focus on Mode T configuration, because of its potential advantages for high efficiency and low cost solar H_2 production in the long term. A detailed comparison and analysis of the two different illumination modes were studied by a recent article [245].

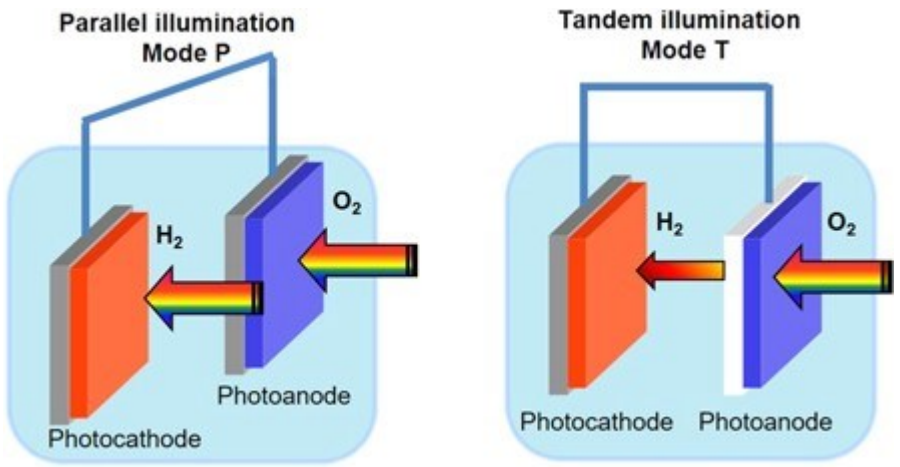

Figure 16. Schematic of PEC tandem cell under parallel (Mode P) and tandem (Mode T) illumination.

Despite promising a high theoretical efficiency up to 30% of the PEC tandem water splitting device, the reported experimental STH efficiency of PEC tandem cells were generally very low (<1%), as listed in table 2. The poor performance of tandem system was largely due to the low photoactivity of the individual photoanode or photocathode. Compared to the water reduction on photocathode, the water oxidation on photoanode is more kinetically challenging due to the complicated four-electron transfer process. A number of studies used TiO_2 or $SrTiO_3$ as the photoanode, due to their excellent stability and large produced photovoltage, to couple with p-GaP [246–248], $CuTiO_x$ [249] or Si-based [250–252] photocathode. However, the efficiencies are very low (<1%), which are largely due to the wide bandgap of photoanode material (>3.0 eV) to match with the solar spectrum. Consequently, various visible-light-responsive photoanode, including WO_3 [55, 253–255], $BiVO_4$ [256–261] and Fe_2O_3 [157, 253], were studied to enhance the light harvesting and current matching with photocathode. Limited success has been achieved with WO_3-based PEC tandem cell, due to the relatively large bandgap of WO_3 (2.8 eV) and the unfavorable conduction band position with respect to the hydrogen evolution potential [55, 253–255]. In contrast, $BiVO_4$ has emerged as the high-performance photoanode material to construct the PEC tandem device, largely due to its relatively negative onset potential (0.2–0.3 V versus RHE) compared to other visible-light responsive oxide-based photoanodes. Bornoz et al coupled $BiVO_4$ photoanode with Cu_2O photocathode as a tandem cell for unassisted solar water splitting [256]. Despite promising a maximum theoretical STH efficiency of 8% based on the current matching approach, a STH efficiency of 0.5% was demonstrated on this alloxide tandem system, which is largely due to the low performance of the individual

electrodes and transmission loss from the front $BiVO_4$ layer. $BiVO_4$ was also combined with high-performance InP [257], Cu-based chalcogenides photocathode, such as $(CuGa)_{0.5}ZnS_2$ [258] and (Ag, Cu)$GaSe_2$ [259], or Si-based photocathode [260, 261]. However, the system exhibited a low efficiency of <1%, which is largely limited by the low performance of photoanode, particularly in the low bias region.

Table 2. Performance comparison of different PEC tandem devices of photoanode–photocathode combinations for solar water splitting.

Photoanode	Photocathode	STH (%)	Stability	Electrolyte	Reference

TiO_2	GaP	N/A	Unstable	1 M NaOH	[246]
TiO_2	GaP	0.25	N/A	0.2 M H_2SO_4	[247]
TiO_2	GaP	0.098	Unstable	1 M NaOH	[248]
TiO_2	$CuTiO_x$	0.3	4–5 h, stable	KOH/Pi	[249]
IrO_x/TiO_2	Pt/Si	0.12	1.5 h, 30% loss	0.5 M H_2SO_4	[250]
TiO_2	$Fe_2O_3/TiO_2/Si$	0.18	N/A	Na2SO4/Pi (pH 7)	[251]
TiO_2	np^+Si	0.39	24 h, 15% loss	1 M KOH	[252]
$SrTiO_3$	GaP	0.67	10 h, stable	1 M NaOH	[248]
WO_3	$GaInP_2$	0.0025	N/A	3 M H_2SO_4	[253]
WO_3	NiO_x/Cu_2O	0.04	Unstable	Na_2SO_4 (pH 6)	[55]
WO_3	Pt/n^+p Si	0.15	10 min, stable	KH_2PO_4 (pH 7)	[254]
WO_3/FTO/p^+n Si	$Pt/TiO_2/Ti/n^+p$ Si	0.24	> 20 h stable	1 M $HClO_4$	[255]
Co–Pi/W:$BiVO_4$	RuO_x/TiO_2/Al:ZnO/Cu_2O	0.5	5000 s, 90% loss,	Na2SO4/Pi (pH 6)	[256]
Co–Pi/$BiVO_4$	Pt/TiO_2/Zn-InP	0.5	N/A	Pi (pH 7)	[257]
$CoO_x/BiVO_4$	$Ru/(CuGa)_{0.5}ZnS_2$	0.016	7 h stable	Pi (pH 8)	[258]
Photoanode	Photocathode	STH (%)	Stability	Electrolyte	Reference

NiOOH/FeOOH /Mo:$BiVO_4$	Pt/CdS/$CuGa_3Se_5$/(Ag, Cu)$GaSe_2$	0.67	2 h stable	Pi (pH 7)	[259]
$CoO_x/TiO_2/BiVO_4$	NiO/$Ni(OH)_2/TiO_2$/Si	0.05	5 h, 50% loss	Bi/K_2SO_4 (pH 9.2)	[260]
Co–Pi/Mo:$BiVO_4$	Pt/Si	0.57	3.5 h, 74% loss	Pi (pH 5.5)	[261]
Fe_2O_3	$GaInP_2$	0.00022	N/A	KNO_3/Pi(pH 5.7)	[253]
$NiFeO_x/Fe_2O_3$	Pt/a-Si	0.91	10 h stable	Pi (pH 11.8)	[157]
$IrO_x/ZnS/CdS/TiO_2$	CdSe/NiO	0.17	20 min, 30% loss	0.5 M Na_2SO_4	[267]
CdS/ZnO	Cu_2S/Cu_2O	0.38	1 h, 90% loss	0.5 M Na_2SO_4	[268]

Although $BiVO_4$ has been set as the case example for photoanode material, it is noteworthy that it suffers from an intrinsic limitation of relatively large bandgap (indirect ~2.4–2.5 eV and direct ~2.7 eV) [262, 263], corresponding to a maximum of ~9% STH effciency that can be theoretically achieved [264]. In addition, $BiVO_4$ is only chemically stable at near neutral condition and dissolves in strong basic and acidic solutions, which make the operating conditions of $BiVO_4$ incompatible with some high-performance catalyst or photocathode conduct optimally only under basic or acidic conditions. Moreover, the buildup of significant pH gradient near the electrode surfaces in neutral solution even with the assistance of additional supporting electrolytes or buffers would fundamentally limit the efficiency [265, 266]. Alternatively, Fe_2O_3 has attracted much interest due to its favorable properties such as relatively narrow bandgap (2.0–2.2 eV), adequate stability in strong alkaline solution, and earth abundance composition. Wang et al paired Fe_2O_3 photoanode with InGaP photocathode as a tandem cell for unassisted water splitting, however, the device performance is extremely low (~0.0002%), which is largely due to the high requisite overpotential of ~0.8 V and low performance of Fe_2O_3 photoanode [253]. Recently, Jang et al reported a benchmark Fe_2O_3 onset potential around 0.45 V versus RHE using a facile regrowth strategy to reduce surface disorders, which enabling unassisted solar water splitting when pairing with an amorphous Si photocathode (figure 17) [157]. A meaningful efficiency of 0.91% and long-term stability of 10 h was achieved by the tandem system based on hematite and Si, which are both earth-abundant.

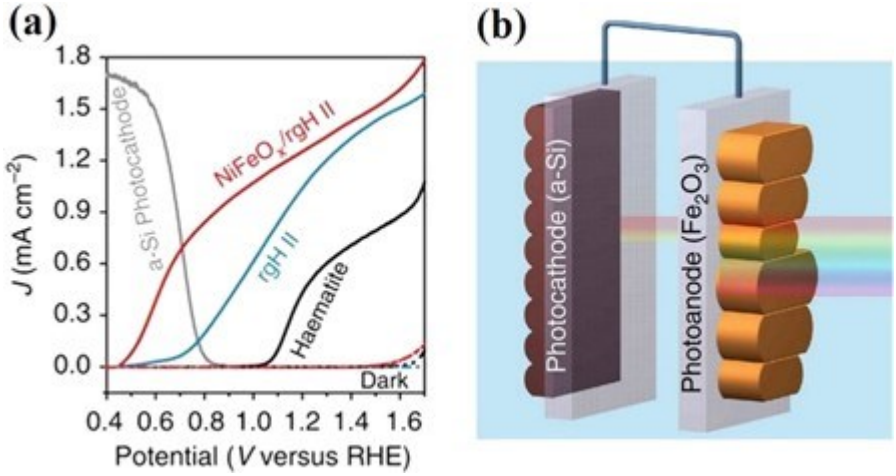

Figure 17. (a) Steady-state current density-potential behaviors of various hematite photoelectrodes. The current densities of Si photocathode placed behind the hematite photoanode are shown to illustrate the meeting points. rgH II denotes hematite samples subjected to the regrowth treatments two times. (b) Schematics of overall unassisted water splitting by hematite photoanode (right) and amorphous Si photocathode (left) in a tandem configuration. Reproduced from [157]. CC BY 4.0.

Compared to metal oxide materials, there are also some examples of PEC tandem device using chalcogenide [267, 268] and nitride-based [269] photoanodes. For example, Yang et al developed a tandem cell composed of CdS quantum dot (QD) modified TiO_2 nanorod photoanode and a CdSe QD modified NiO nanosheet photocathode, obtaining a STH efficiency of 0.17% [267]. With the assistance of a ZnS passivation layer and an IrO_x OER co-catalyst, the device efficiency and stability were greatly enhanced. In another study, AlOtaibi et al designed a PEC tandem cell consisting of GaN/InGaN nanowire photoanodes and a Si/InGaN nanowire photocathode, which achieved a high STH efficiency of 1.5% in 1 M HBr [269]. The distinct advantage of nanowire photoelectrodes, together with the parallel illumination strategy by splitting the solar spectrum spatially and spectrally, enhanced the solar energy conversion efficiency for unassisted water splitting.

4. Conclusions and outlook

Artificial photosynthesis via solar water splitting, which mimics the natural photosynthesis, is a promising approach to directly convert sunlight into energy-rich chemical fuel (i.e. H_2) on a global scale. The light-harvesting semiconductor material, as an artificial leaf, plays an

essential role in determining the performance of artificial photosynthesis devices. Recently, three parallel approaches have been pursued to achieve a material system with both high efficiency and robust stability: (i) making stable materials more efficient, (ii) enabling efficient materials are more stable, and (iii) discovering new materials that are intrinsically stable and highly efficient.

Metal oxides are generally reported to be very stable and exhibit a high-level resistance to photocorrosion. But they usually suffer from relatively large bandgap and low absorption coefficient, poor electrical conductivity, short charge carrier lifetime and diffusion length, which significantly limit the performance. For example, the optical absorption depths of metal oxides (usually hundreds of nanometers) are often larger than the hole diffusion lengths (e.g. less than 5 and 20 nm for Fe_2O_3 and TiO_2, respectively) [270]. Nanostructuring techniques such as the fabrication of nanowires, nanotubes or nanopores can alleviate this issue by shortening the carrier diffusion distance toward the electrolyte solution. Recently, this strategy has been demonstrated with remarkable success in the case of $BiVO_4$ photoanode, together with other strategies such as doping and co-catalyst modification [271]. Using $BiVO_4$ as a model case, it is highly desirable to apply similar strategies on other metal oxides with a lower bandgap (<2.4 eV), both as photoanodes and photocathodes, to achieve the goal of STH efficiency >10%.

Si, III–V and chalcopyrite semiconductors, which usually have a narrow bandgap and can be obtained with high-quality (relatively low defects, low impurity incorporation, and high controllability of doping), have been reported with high efficiency for water splitting. However, they are chemically unstable and suffer from photocorrosion when directly in contact with an aqueous electrolyte solution. Recent developments on surface protection technology greatly improve the stability of these classic PV materials by decoupling the light absorption sites with electrochemical reaction sites [272, 273]. Metal oxides such as TiO_2 are extensively used as the protection layers owing to the high stability over a wide range of pH and excellent optical transmittance (E_g > 3.0 eV). ALD technique, which allows for conformal coating with precisely controlled thickness, has been demonstrated with great success for achieving high stability solar water splitting system [274], e.g. over 2200 h stable operation has been proved on Si-based photoanode with an ALD-TiO_2 protection layer [275]. A similar concept can also be pursued using simple, cost-effective and scalable protection approaches (e.g. solution-based sol-gel and chemical bath) [276]. It is worth noting that the parasitic light absorption from the protection layer needs not to be

considered in the case of the bottom absorber, which allows the wide choice of protection materials such as metals.

Recently, nitrides, TMDs and organic materials have emerged as promising photoelectrodes for water splitting due to their unique optoelectronic properties. For example, InGaN is the only known semiconductor material whose bandgap can straddle the redox potentials of water splitting under deep visible and near-infrared light irradiation [84]. Nearly two orders of magnitude enhancement in the quantum efficiency for photocatalytic overall water splitting on (In)GaN nanowires has been demonstrated [77, 78]. Unique to such III-nitride nanowire structures synthesized by molecular beam epitaxy is the presence of a Ntermination, not only for their $(000\bar{1})$ top faces but also for their $(10\bar{1}0)$ side faces [85]. The Ntermination of all exposed surfaces (top-polar and side-nonpolar) protects the nanowires against attack by the electrolyte (oxidation and photocorrosion). Although the studies of these emerged materials are still in the early stage, they have already shown great promise. Further developments will enable their great success. In parallel, it is important to discover other new materials that are intrinsically stable and with favorable optoelectronic properties for PEC water splitting (e.g. suitable bandgap and high charge carrier mobility). For example, 8000 and 700 000 compound materials are available for ternary and quaternary metal oxides respectively, with most of them are yet to be investigated for PEC water splitting [277]. The large number of untested elemental combinations gives hope that ideal materials are still ahead of us. Applying advanced combinational methods, as well as the state-of-the-art theoretical calculations to potential complex materials will be crucial for speeding up the discovery of high-performance photoelectrodes for water splitting.

To achieve efficient and cost-effective unassisted solar water splitting, a PEC tandem device consisting of a photoanode and photocathode is a promising configuration. The theoretical modeling of using a combination of 1.6–1.8 eV top absorber and 0.9–1.2 eV bottom absorber to achieve high efficiency has been validated using high-quality III–V materials. By tuning the bandgap combination, benchmarking STH efficiencies of 16% and 19% were reported in a monolithic 1.8/1.2 eV GaInP/GaInAs tandem device from Deutsch's group [29] and Atwater's group [278], respectively. Further improvement of STH efficiency towards >20% is possible using a 1.7/1.1 eV optimal bandgap combination. Si is nearly ideal as the bottom light absorber in the tandem device owing to its energy bandgap of 1.1 eV, earth abundance, and prevalence in PV industry. By controlled doping with P and B, Si can be fabricated with n-type and p-type as photoanode and photocathode, respectively. The PEC performance of state-of-the-art Si-based photoanode and photocathode with a single

junction are shown in figure 18. To pair with the Si photocathode, $BiVO_4$ is currently the best photoanode in terms of operating current density. Developing a low-bandgap photoanode close to 1.7 eV that gives higher photocurrent at the low bias region (e.g. below 0.6 V versus RHE) would be highly desired. To couple with the Si photoanode, there is still no prominent photocathode that can give a meaningful operating point. High-performance photocathodes including InP, due to the low produced photovoltage, are not able to intersect with the Si photoanode. Recently, a positive onset potential of >1 V versus RHE was obtained on Cu_2O [61] and $CuBi_2O_4$-based photocathodes [68, 69]. However, the photocurrent performance of the photocathodes is relatively low. Efforts therefore are needed to develop a photocathode that can deliver high photocurrent at a positive potential (e.g. above 0.9 V versus RHE) for constructing efficient tandem device with Si photoanode. Owing to their bandgap tenability, suitable band edge positions, high material quality and well-controlled doping to achieve n-type or p-type, III–V semiconductors can potentially overcome the efficiency bottleneck that are commonly seen by other materials. The integration of III–V materials, particularly III-nitride nanostructures with Si, largely leverages the well-established semiconductor manufacturing processes (e.g. solid-state lighting and power electronics) with low cost and large area Si solar cell platform, which promises a viable approach for large-scale solar hydrogen production from water splitting.

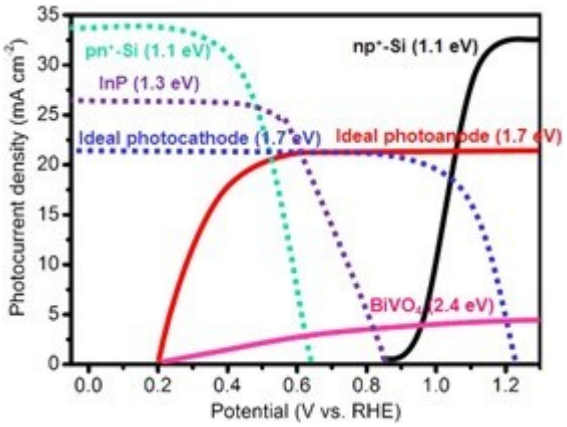

Figure 18. J–V curves of state-of-the-art p–n^+ Si-based photocathode [124], n–p^+ Si-based photoanode [221], InP-based photocathode [74] and $BiVO_4$-based photoanode [162] to construct a PEC tandem device based on Si bottom cell. The J–V curves of the ideal photocathode and photoanode are also projected. Note that the

parasitic light absorption from the top light absorber and current match condition between the top and bottom light absorber should be taken into account in the real tandem device.

References

[1] Walter M G, Warren E L, McKone J R, Boettcher S W, Mi Q X, Santori E A and Lewis N S 2010 Solar water splitting cells Chem. Rev. 110 6446 Crossref

[2] Luo J, Im J-H, Mayer M T, Schreier M, Nazeeruddin M K, Park N-G, Tilley S D, Fan H J and Grätzel M 2014 Water photolysis at 12.3% efficiency via perovskite photovoltaics and earthabundant catalysts Science 345 1593 Crossref

[3] Nakamura A, Ota Y, Koike K, Hidaka Y, Nishioka K, Sugiyama M and Fujii K 2015 A 24.4% solar to hydrogen energy conversion efficiency by combining concentrator photovoltaic modules and electrochemical cells Appl. Phys. Express 8 107101 IOPscience (http://iopscience.iop.org/1882-0786/8/10/107101)

[4] Cox C R, Lee J Z, Nocera D G and Buonassisi T 2014 Ten-percent solar-to-fuel conversion with nonprecious materials Proc. Natl Acad. Sci. 111 14057 Crossref

[5] Jacobsson T J, Fjällström V, Sahlberg M, Edoff M and Edvinsson T 2013 A monolithic device for solar water splitting based on series interconnected thin film absorbers reaching over 10% solar-to-hydrogen efficiency Energy Environ. Sci. 6 3676 Crossref

[6] Peharz G, Dimroth F and Wittstadt U 2007 Solar hydrogen production by water splitting with a conversion efficiency of 18% Int. J. Hydrog. Energy 32 3248 Crossref

[7] Licht S, Wang B, Mukerji S, Soga T, Umeno M and Tributsch H 2001 Over 18% solar energy conversion to generation of hydrogen fuel; theory and experiment for efficient solar water splitting Int. J. Hydrog. Energy 26 653 Crossref

[8] Khaselev O, Bansal A and Turner J 2001 High-efficiency integrated multijunction photovoltaic/electrolysis systems for hydrogen production Int. J. Hydrog. Energy 26 127 Crossref

[9] Jia J Y, Seitz L C, Benck J D, Huo Y J, Chen Y S, Ng J W D, Bilir T, Harris J S and Jaramillo T F

2016 Solar water splitting by photovoltaic-electrolysis with a solar-to-hydrogen efficiency over30% Nat. Commun. 7 13237 Crossref

[10] Nowotny J, Bak T, Chu D W, Fiechter S, Murch G E and Veziroglu T N 2014 Sustainable practices: solar hydrogen fuel and education program on sustainable energy systems Int. J. Hydrog. Energy 39 4151
Crossref

[11] Fabian D M, Hu S, Singh N, Houle F A, Hisatomi T, Domen K, Osterlohf F E and Ardo S 2015 Particle suspension reactors and materials for solar-driven water splitting Energy Environ. Sci. 8 2825
Crossref

[12] Ager J W, Shaner M R, Walczak K A, Sharp I D and Ardo S 2015 Experimental demonstrations of spontaneous, solar-driven photoelectrochemical water splitting Energy Environ. Sci. 8 2811
Crossref

[13] McKone J R, Lewis N S and Gray H B 2014 Will solar-driven water-splitting devices see the light of day? Chem. Mater. 26 407 Crossref

[14] Pinaud B A et al 2013 Technical and economic feasibility of centralized facilities for solar hydrogen production via photocatalysis and photoelectrochemistry Energy Environ. Sci. 6 1983
Crossref

[15] Shaner M R, Atwater H A, Lewis N S and McFarland E W 2016 A comparative technoeconomic analysis of renewable hydrogen production using solar energy Energy Environ. Sci. 9 2354
Crossref

[16] Sathre R, Scown C D, Morrow W R, Stevens J C, Sharp I D, Ager J W, Walczak K, Houle F A and Greenblatt J B 2014 Life-cycle net energy assessment of large-scale hydrogen production via photoelectrochemical water splitting Energy Environ. Sci. 7 3264 Crossref

[17] Hisatomi T and Domen K 2017 Introductory lecture: sunlight-driven water splitting and carbon dioxide reduction by heterogeneous semiconductor systems as key processes in artificial photosynthesis Faraday Discuss. 198 11 Crossref

[18] Prevot M S and Sivula K 2013 Photoelectrochemical tandem cells for solar water splitting J. Phys. Chem. C 117 17879
Crossref

[19] Zhang K, Ma M, Li P, Wang D H and Park J H 2016 Water splitting progress in tandem devices: moving photolysis beyond electrolysis Adv. Energy Mater. 6 1600602 Crossref

[20] Ross R T and Hsiao T L 1977 Limits on the yield of photochemical solar energy conversion J. Appl. Phys. 48 4783 Crossref

[21] Nozik A J 1977 Photochemical diodes Appl. Phys. Lett. 30 567 Crossref

[22] Weber M F and Dignam M J 1984 Efficiency of splitting water with semiconducting photoelectrodes J. Electrochem. Soc. 131 1258 Crossref

[23] Bolton J R, Strickler S J and Connolly J S 1985 Limiting and realizable efficiencies of solar photolysis of water Nature 316 495 Crossref

[24] Haussener S, Hu S, Xiang C, Weber A Z and Lewis N S 2013 Simulations of the irradiation and temperature dependence of the efficiency of tandem photoelectrochemical watersplitting systems Energy Environ. Sci. 6 3605 Crossref

[25] Hu S, Xiang C, Haussener S, Berger A D and Lewis N S 2013 An analysis of the optimal band gaps of light absorbers in integrated tandem photoelectrochemical water-splitting systems Energy Environ. Sci. 6 2984 Crossref

[26] Döscher H, Geisz J F, Deutsch T G and Turner J A 2014 Sunlight absorption in water—efficiency and design implications for photoelectrochemical devices Energy Environ. Sci. 7 2951

Crossref

[27] Seitz L C, Chen Z, Forman A J, Pinaud B A, Benck J D and Jaramillo T F 2014 Modeling practical performance limits of photoelectrochemical water splitting based on the current state of materials research ChemSusChem 7 1372 Crossref

[28] Fountaine K T, Lewerenz H J and Atwater H A 2016 Efficiency limits for photoelectrochemical water-splitting Nat. Commun. 7 13706 Crossref

[29] Young J L, Steiner M A, Döscher H, France R M, Turner J A and Deutsch Todd G 2017 Direct solar-to-hydrogen conversion via inverted metamorphic multi-junction semiconductor architectures Nat. Energy 2 17028 Crossref

[30] Seger B, Hansen O and Vesborg P C K 2017 A flexible web-based approach to modeling tandem photocatalytic devices Sol. RRL 1 e201600013 Crossref

[31] Montoya J H, Seitz L C, Chakthranont P, Vojvodic A, Jaramillo T F and Norskov J K 2017 Materials for solar fuels and chemicals Nat. Mater. 16 70 Crossref

[32] Peter W and Uli W 2016 Physics of Solar Cells: From Basic Principles to Advanced Concepts (New York: Wiley)

[33] Lewis N S 2005 Chemical control of charge transfer and recombination at semiconductor photoelectrode surfaces Inorg. Chem. 44 6900 Crossref

[34] Dirnstorfer I, Simon D K, Jordan P M and Mikolajick T 2014 Near surface inversion layer recombination in Al2O3 passivated n-type silicon J. Appl. Phys. 116 044112 Crossref

[35] Sze S M and Ng K K 2006 Physics of Semiconductor Devices (New York: Wiley) Crossref

[36] Peter L M 2016 Photoelectrochemistry: from basic principles to photocatalysis Photocatalysis: Fundamentals and Perspectives (Cambridge: The Royal Society of Chemistry) ch 1

Crossref

[37] Tan M X, Kenyon C N, Krüger O and Lewis N S 1997 Behavior of Si photoelectrodes under high level injection conditions: I. Steady-state current–voltage properties and quasi-Fermi level positions under illumination J. Phys. Chem. B 101 2830 Crossref

[38] Krüger O, Kenyon C N, Tan M X and Lewis N S 1997 Behavior of Si photoelectrodes under high level injection conditions: II. Experimental measurements and digital simulations of the behavior of quasi-Fermi levels under illumination and applied bias J. Phys. Chem. B 101 2840
Crossref

[39] Kenyon C N, Tan M X, Krüger O and Lewis N S 1997 Behavior of Si photoelectrodes under high level injection conditions: III. Transient and steady-state measurements of the quasiFermi levels at Si/CH3OH contacts J. Phys. Chem. B 101 2850 Crossref

[40] Du C, Yang X, Mayer M T, Hoyt H, Xie J, McMahon G, Bischoping G and Wang D 2013 Hematite-based water splitting with low turn-on voltages Angew. Chem., Int. Ed. Engl. 52 12692
Crossref

[41] Landsberg P T 2003 Recombination in Semiconductors (Cambridge: Cambridge University Press)

[42] Giménez S and Bisquert J 2016 Photoelectrochemical Solar Fuel Production (Berlin: Springer)
Crossref

[43] Peter L M, Li J and Peat R 1984 Surface recombination at semiconductor electrodes J. Electroanal. Chem. Interfacial Electrochem. 165 29 Crossref

[44] Reichman J 1980 The current–voltage characteristics of semiconductor-electrolyte junction photovoltaic cells Appl. Phys. Lett. 36 574 Crossref

[45] El Guibaly F, Colbow K and Funt B L 1981 Voltage dependence of the dark and photocurrents in semiconductor–electrolyte junctions J. Appl. Phys. 52 3480

[46] El Guibaly F and Colbow K 1982 Theory of photocurrent in semiconductor-electrolyte junction solar cells J. Appl. Phys. 53 1737 Crossref

[47] Sivula K and van de Krol R 2016 Semiconducting materials for photoelectrochemical energy conversion Nat. Rev. Mater. 1 15010 Crossref

[48] Paracchino A, Brauer J C, Moser J E, Thimsen E and Graetzel M 2012 Synthesis and characterization of high-photoactivity electrodeposited Cu2O solar absorber by photoelectrochemistry and ultrafast spectroscopy J. Phys. Chem. C 116 7341 Crossref

[49] Meyer B K et al 2012 Binary copper oxide semiconductors: from materials towards devices Phys. Status Solidi b 249 1487 Crossref

[50] Paracchino A, Laporte V, Sivula K, Gratzel M and Thimsen E 2011 Highly active oxide photocathode for photoelectrochemical water reduction Nat. Mater. 10 456 Crossref

[51] Azevedo J, Tilley S D, Schreier M, Stefik M, Sousa C, Araujo J P, Mendes A, Gratzel M and Mayer M T 2016 Tin oxide as stable protective layer for composite cuprous oxide watersplitting photocathodes Nano Energy 24 10 Crossref

[52] Dias P et al 2015 Transparent cuprous oxide photocathode enabling a stacked tandem cell for unbiased water splitting Adv. Energy Mater. 5 1501537 Crossref

[53] Huang Q, Kang F, Liu H, Li Q and Xiao X D 2013 Highly aligned Cu2O/CuO/TiO2 core/shell nanowire arrays as photocathodes for water photoelectrolysis J. Mater. Chem. A 1 2418 Crossref

[54] Dubale A A, Tamirat A G, Chen H M, Berhe T A, Pan C J, Su W N and Hwang B J 2016 A highly stable CuS and CuS-Pt modified Cu2O/CuO heterostructure as an efficient photocathode for the hydrogen evolution reaction J. Mater. Chem. A 4 2205 Crossref

[55] Lin C Y, Lai Y H, Mersch D and Reisner E 2012 Cu2O vertical bar NiOx nanocomposite as an inexpensive photocathode in photoelectrochemical water splitting Chem. Sci. 3 3482 Crossref

[56] Minami T, Miyata T and Nishi Y 2014 Cu2O-based heterojunction solar cells with an Al-doped ZnO/oxide semiconductor/thermally oxidized Cu2O sheet structure Sol. Energy 105 206 Crossref

[57] Chang K, Mei Z W, Wang T, Kang Q, Ouyang S X and Ye J H 2014 MoS2/graphene cocatalyst for efficient photocatalytic H2 evolution under visible light irradiation ACS Nano 8 7078 Crossref

Crossref

[58] Tilley S D, Schreier M, Azevedo J, Stefik M and Graetzel M 2014 Ruthenium oxide hydrogen evolution catalysis on composite cuprous oxide water-splitting photocathodes Adv. Funct. Mater. 24 303
Crossref

[59] Morales-Guio C G, Tilley S D, Vrubel H, Gratzel M and Hu X L 2014 Hydrogen evolution from a copper(I) oxide photocathode coated with an amorphous molybdenum sulphide catalyst Nat. Commun. 5 3059
Crossref

[60] Luo J S, Steier L, Son M K, Schreier M, Mayer M T and Gratzel M 2016 Cu2O nanowire photocathodes for efficient and durable solar water splitting Nano Lett. 16 1848 Crossref

[61] Li C L, Hisatomi T, Watanabe O, Nakabayashi M, Shibata N, Domen K and Delaunay J J 2015 Positive onset potential and stability of Cu2O-based photocathodes in water splitting by atomic layer deposition of a Ga2O3 buffer layer Energy Environ. Sci. 8 1493 Crossref

[62] Read C G, Park Y and Choi K S 2012 Electrochemical synthesis of p-type CuFeO2 electrodes for use in a photoelectrochemical cell J. Phys. Chem. Lett. 3 1872 Crossref

[63] Jang Y J, Park Y B, Kim H E, Choi Y H, Choi S H and Lee J S 2016 Oxygen-intercalated CuFeO2 photocathode fabricated by hybrid microwave annealing for efficient solar hydrogen production Chem. Mater. 28 6054 Crossref

[64] Prevot M S, Guijarro N and Sivula K 2015 Enhancing the performance of a robust sol-gelprocessed p-type delafossite CuFeO2 photocathode for solar water reduction ChemSusChem 8 1359

[65] Arai T, Konishi Y, Iwasaki Y, Sugihara H and Sayama K 2007 High-throughput screening using porous photoelectrode for the development of visible-light-responsive semiconductors J. Comb. Chem. 9 574
Crossref

[66] Hahn N T, Holmberg V C, Korgel B A and Mullins C B 2012 Electrochemical synthesis and characterization of p-CuBi2O4 thin film photocathodes J. Phys. Chem. C 116 6459 Crossref

[67] Cao D W, Nasori N, Wang Z J, Mi Y, Wen L Y, Yang Y, Qu S C, Wang Z G and Lei Y 2016 p-Type CuBi2O4: an easily accessible photocathodic material for high-efficiency water splitting J. Mater. Chem. A 4 8995
Crossref

[68] Berglund S P, Abdi F F, Bogdanoff P, Chernseddine A, Friedrich D and van de Krol R 2016 Comprehensive evaluation of CuBi2O4 as a photocathode material for photoelectrochemical water splitting Chem. Mater. 28 4231 Crossref

[69] Kang D, Hill J C, Park Y and Choi K S 2016 Photoelectrochemical properties and photostabilities of high surface area CuBi2O4 and Ag-doped CuBi2O4 photocathodes Chem. Mater. 28 4331
Crossref

[70] Green M A, Hishikawa Y, Warta W, Dunlop E D, Levi D H, Hohl-Ebinger J and Ho-Baillie A W H 2017 Solar cell efficiency tables (version 50) Prog. Photovolt., Res. Appl. 25 668 Crossref

[71] Siddiqi G, Pan Z and Hu S 2017 III–V semiconductor photoelectrodes Semiconduct. Semimet. 97 81
Crossref

[72] Lee M H et al 2012 p-type InP nanopillar photocathodes for efficient solar-driven hydrogen production Angew. Chem., Int. Ed. Engl. 51 10760 Crossref

[73] Lin Y J et al 2015 Role of TiO2 surface passivation on improving the performance of p-InP photocathodes J. Phys. Chem. C 119 2308 Crossref

[74] Gao L et al 2016 High-efficiency InP-based photocathode for hydrogen production by interface energetics design and photon management Adv. Funct. Mater. 26 679

Crossref

[75] Wang D, Pierre A, Kibria M G, Cui K, Han X G, Bevan K H, Guo H, Paradis S, Hakima A R and Mi Z 2011 Wafer-level photocatalytic water splitting on gan nanowire arrays grown by molecular beam epitaxy Nano Lett. 11 2353 Crossref

[76] Kibria M G, Nguyen H P T, Cui K, Zhao S R, Liu D P, Guo H, Trudeau M L, Paradis S, Hakima A
R and Mi Z 2013 One-step overall water splitting under visible light using multiband InGaN/GaN nanowire heterostructures ACS Nano 7 7886 Crossref

[77] Kibria M G, Chowdhury F A, Zhao S, AlOtaibi B, Trudeau M L, Guo H and Mi Z 2015 Visible light-driven efficient overall water splitting using p-type metal-nitride nanowire arrays Nat.

Crossref

Commun. 6 6797
Crossref

[78] Kibria M G, Zhao S, Chowdhury F A, Wang Q, Nguyen H P T, Trudeau M L, Guo H and Mi Z 2014 Tuning the surface Fermi level on p-type gallium nitride nanowires for efficient overall water splitting Nat. Commun. 5 3825 Crossref

[79] Chowdhury F A, Mi Z, Kibria M G and Trudeau M L 2015 Group III-nitride nanowire structures for photocatalytic hydrogen evolution under visible light irradiation APL Mater. 3 104408 Crossref

[80] Kibria M G and Mi Z 2016 Artificial photosynthesis using metal/nonmetal-nitride semiconductors: current status, prospects, and challenges J. Mater. Chem. A 4 2801 Crossref

[81] Chu S, Kong X, Vanka S, Guo H and Mi Z 2017 Artificial photosynthesis on III-nitride nanowire arrays Semiconduct. Semimet. 97 223 Crossref

[82] Jung H S, Hong Y J, Li Y, Cho J, Kim Y J and Yi G C 2008 Photocatalysis using GaN nanowires ACS Nano 2 637
Crossref

[83] Moustakas T D 2013 The role of extended defects on the performance of optoelectronic devices in nitride semiconductors Phys. Status Solidi a 210 169

[84] Moses P G and Van de Walle C G 2010 Band bowing and band alignment in InGaN alloys Appl. Phys. Lett. 96 021908
Crossref

[85] Kibria M G et al 2016 Atomic-scale origin of long-term stability and high performance of pGaN nanowire arrays for photocatalytic overall pure water splitting Adv. Mater. 28 8388 Crossref

[86] Fujii K and Ohkawa K 2005 Photoelectrochemical properties of p-type GaN in comparison with n-type GaN Japan. J. Appl. Phys. 44 L909
IOPscience (http://iopscience.iop.org/1347-4065/44/7L/L909)

[87] Aryal K, Pantha B N, Li J, Lin J Y and Jiang H X 2010 Hydrogen generation by solar water splitting using p-InGaN photoelectrochemical cells Appl. Phys. Lett. 96 052110 Crossref

[88] Fan S Z, AlOtaibi B, Woo S Y, Wang Y J, Botton G A and Mi Z 2015 High efficiency solar-tohydrogen conversion on a monolithically integrated InGaN/GaN/Si adaptive tunnel junction photocathode Nano Lett. 15 2721 Crossref

[89] Alonso M I, Wakita K, Pascual J, Garriga M and Yamamoto N 2001 Optical functions and electronic structure of CuInSe2, CuGaSe2, CuInS2, and CuGaS2 Phys. Rev. B 63 075203 Crossref

[90] Chen S Y, Yang J H, Gong X G, Walsh A and Wei S H 2010 Intrinsic point defects and complexes in the quaternary kesterite semiconductor Cu2ZnSnS4 Phys. Rev. B 81 245204 Crossref

[91] Zhang S B, Wei S H, Zunger A and Katayama-Yoshida H 1998 Defect physics of the CuInSe2 chalcopyrite semiconductor Phys. Rev. B 57 9642 Crossref

[92] Wei S H and Zhang S B 2005 Defect properties of CuInSe2 and CuGaSe2 J. Phys. Chem. Solids 66 1994
Crossref

[93] Bar M, Bohne W, Rohrich J, Strub E, Lindner S, Lux-Steiner M C, Fischer C H, Niesen T P and
Karg F 2004 Determination of the band gap depth profile of the penternary Cu(In(1−X)GaX)(SYSe(1−Y))2 chalcopyrite from its composition gradient J. Appl. Phys. 96 3857 Crossref

Crossref

[94] Raulot J M, Domain C and Guillemoles J F 2005 Ab initio investigation of potential indium and gallium free chalcopyrite compounds for photovoltaic application J. Phys. Chem. Solids 66 2019
Crossref

[95] Jaffe J E and Zunger A 1984 Theory of the band-gap anomaly in ABC2 chalcopyrite semiconductors Phys. Rev. B 29 1882 Crossref

[96] Chen S Y, Gong X G, Walsh A and Wei S H 2010 Defect physics of the kesterite thin-film solar cell absorber Cu2ZnSnS4 Appl. Phys. Lett. 96 021902 Crossref

[97] Assoud A, Soheilnia N and Kleinke H 2005 New quaternary barium copper/silver selenostannates: different coordination spheres, metal–metal interactions, and physical properties Chem. Mater. 17 2255 Crossref

[98] Hong F, Lin W J, Meng W W and Yan Y F 2016 Trigonal Cu2-II-Sn-VI4 (II = Ba, Sr and VI = S, Se) quaternary compounds for earth-abundant photovoltaics Phys. Chem. Chem. Phys. 18 4828
Crossref

[99] Xiao Z W, Meng W W, Li J V and Yan Y F 2017 Distant-atom mutation for better earthabundant light absorbers: a case study of Cu2BaSnSe4 ACS Energy Lett. 2 29 Crossref

[100] Shin D, Saparov B, Zhu T, Huhn W P, Blum V and Mitzi D B 2016 BaCu2Sn(S, Se)4: earthabundant chalcogenides for thin-film photovoltaics Chem. Mater. 28 4771 Crossref

[101] Marsen B, Cole B and Miller E L 2008 Photoelectrolysis of water using thin copper gallium diselenide electrodes Sol. Energy Mater. Sol. Cells 92 1054 Crossref

[102] Moriya M, Minegishi T, Kumagai H, Katayama M, Kubota J and Domen K 2013 Stable hydrogen evolution from CdS-modified CuGaSe2 photoelectrode under visible-light irradiation J. Am. Chem. Soc. 135 3733 Crossref

[103] Gunawan, Septina W, Ikeda S, Harada T, Minegishi T, Domen K and Matsumura M 2014 Platinum and indium sulfide-modified CuInS2 as efficient photocathodes for photoelectrochemical water splitting Chem. Commun. 50 8941 Crossref

[104] Zhao J et al 2014 Enhancement of solar hydrogen evolution from water by surface modification with CdS and TiO2 on porous CuInS2 photocathodes prepared by an electrodeposition-sulfurization method Angew. Chem., Int. Ed. Engl. 53 11808 Crossref

[105] Mali M G, Yoon H, Joshi B N, Park H, Al-Deyab S S, Lim D C, Ahn S, Nervi C and Yoon S S 2015 Enhanced photoelectrochemical solar water splitting using a platinum-decorated CIGS/CdS/ZnO photocathode ACS Appl. Mater. Interfaces 7 21619 Crossref

[106] Kumagai H, Minegishi T, Sato N, Yamada T, Kubota J and Domen K 2015 Efficient solar hydrogen production from neutral electrolytes using surface-modified Cu(In, Ga)Se2 photocathodes J. Mater. Chem. A 3 8300 Crossref

[107] Guan Z J, Luo W J, Feng J Y, Tao Q C, Xu Y, Wen X, Fu G and Zou Z G 2015 Selective etching of metastable phase induced an efficient CuIn0.7Ga0.3S2 nano-photocathode for solar water splitting J. Mater. Chem. A 3 7840 Crossref

[108] Guijarro N, Prevot M S, Yu X Y, Jeanbourquin X A, Bornoz P, Bouree W, Johnson M, Le Formal
F and Sivula K 2016 A bottom-up approach toward all-solution-processed high-efficiency Cu(In, Ga)S2 photocathodes for solar water splitting Adv. Energy Mater. 6 1501949 Crossref

[109] Yokoyama D, Minegishi T, Jimbo K, Hisatomi T, Ma G, Katayama M, Kubota J, Katagiri H and Domen K 2010 H2 evolution from water on modified Cu2ZnSnS4 photoelectrode under solar light Appl. Phys. Express 3 101202
IOPscience (http://iopscience.iop.org/1882-0786/3/10/101202)

[110] Li B J, Yin P F, Zhou Y Z, Gao Z M, Ling T and Du X W 2015 Single crystalline Cu2ZnSnS4 nanosheet arrays for efficient photochemical hydrogen generation RSC Adv. 5 2543 Crossref

[111] Guan Z J, Luo W J, Xu Y, Tao Q C, Wen X and Zou Z G 2016 Aging precursor solution in high humidity remarkably promoted grain growth in Cu2ZnSnS4 films ACS Appl. Mater. Interfaces 8 5432
Crossref

[112] Jiang F, Gunawan, Harada T, Kuang Y B, Minegishi T, Domen K and Ikeda S 2015 Pt/In2S3/CdS/Cu2ZnSnS4 thin film as an efficient and stable photocathode for water reduction under sunlight radiation J. Am. Chem. Soc. 137 13691 Crossref

[113] Ge J, Koirala P, Grice C R, Roland P J, Yu Y, Tan X X, Ellingson R J, Collins R W and Yan Y F
2017 Oxygenated CdS buffer layers enabling high open-circuit voltages in earth-abundantCu2BaSnS4 thin-film solar cells Adv. Energy Mater. 7 1601803 Crossref

[114] Ge J et al 2017 Employing overlayers to improve the performance of Cu2BaSnS4 thin film based photoelectrochemical water reduction devices Chem. Mater. 29 916 Crossref

[115] Ge J, Yu Y and Yan Y F 2016 Earth-abundant trigonal BaCu2Sn(SexS1−x)4 (x = 0–0.55) thin films with tunable band gaps for solar water splitting J. Mater. Chem. A 4 18885 Crossref

[116] Ge J, Yu Y and Yan Y F 2016 Earth-abundant orthorhombic BaCu2Sn(SexS1−x)4 (x approximate to 0.83) thin film for solar energy conversion ACS Energy Lett. 1 583 Crossref

[117] Shin D, Ngaboyamahina E, Zhou Y H, Glass J T and Mitzi D B 2016 Synthesis and characterization of an earth-abundant Cu2BaSn(S, Se)4 chalcogenide for photoelectrochemical cell application J. Phys. Chem. Lett. 7 4554 Crossref

[118] Sun K, Shen S H, Liang Y Q, Burrows P E, Mao S S and Wang D L 2014 Enabling silicon for solar-fuel production Chem. Rev. 114 8662 Crossref

[119] Maier C U, Specht M and Bilger G 1996 Hydrogen evolution on platinum-coated p-silicon photocathodes Int. J. Hydrog. Energy 21 859 Crossref

[120] Seger B, Pedersen T, Laursen A B, Vesborg P C K, Hansen O and Chorkendorff I 2013 Using TiO2 as a conductive protective layer for photocathodic H2 evolution J. Am. Chem. Soc. 135 1057
Crossref

[121] Seger B, Tilley D S, Pedersen T, Vesborg P C K, Hansen O, Gratzel M and Chorkendorff I 2013 Silicon protected with atomic layer deposited TiO2: durability studies of photocathodic

H2 evolution RSC Adv. 3 25902
Crossref

[122] Oh I, Kye J and Hwang S 2012 Enhanced photoelectrochemical hydrogen production from silicon nanowire array photocathode Nano Lett. 12 298 Crossref

[123] Boettcher S W et al 2011 Photoelectrochemical hydrogen evolution using Si microwire arrays J. Am. Chem. Soc. 133 1216 Crossref

[124] Wang H P, Sun K, Noh S Y, Kargar A, Tsai M L, Huang M Y, Wang D L and He J H 2015 Highperformance a-Si/c-Si heterojunction photoelectrodes for photoelectrochemical oxygen and hydrogen evolution Nano Lett. 15 2817 Crossref

[125] Lin Y J, Battaglia C, Boccard M, Hettick M, Yu Z B, Ballif C, Ager J W and Javey A 2013 Amorphous Si thin film based photocathodes with high photovoltage for efficient hydrogen production Nano Lett. 13 5615 Crossref

[126] Yu X and Sivula K 2017 Layered 2D semiconducting transition metal dichalcogenides for solar energy conversion Curr. Opin. Electrochem. 2 97 Crossref

[127] Jariwala D, Sangwan V K, Lauhon L J, Marks T J and Hersam M C 2014 Emerging device applications for semiconducting two-dimensional transition metal dichalcogenides ACS Nano 8 1102
Crossref

[128] Lv R, Robinson J A, Schaak R E, Sun D, Sun Y F, Mallouk T E and Terrones M 2015 Transition metal dichalcogenides and beyond: synthesis, properties, and applications of single- and few-layer nanosheets Acc. Chem. Res. 48 56 Crossref

[129] Baglio J A, Calabrese G S, Harrison D J, Kamienieck E, Ricco A J, Wrighton M S and Zoski G D 1983 Electrochemical characterization of p-type semiconducting tungsten disulfide photocathodes: efficient photoreduction processes at semiconductor/liquid electrolyte interfaces J. Am. Chem. Soc. 105 2246 Crossref

[130] McKone J R, Pieterick A P, Gray H B and Lewis N S 2013 Hydrogen evolution from Pt/Rucoated p-type WSe2 photocathodes J. Am. Chem. Soc. 135 223 Crossref

[131] Haro M, Solis C, Blas-Ferrando V M, Margeat O, Ben Dhkil S, Videlot-Ackermann C, Ackermann J, Di Fonzo F, Guerrero A and Gimenez S 2016 Direct hydrogen evolution from saline water reduction at neutral pH using organic photocathodes ChemSusChem 9 3062 Crossref

[132] Queyriaux N, Kaeffer N, Morozan A, Chavarot-Kerlidou M and Artero V 2015 Molecular cathode and photocathode materials for hydrogen evolution in photoelectrochemical devices J. Photochem. Photobiol. C 25 90 Crossref

[133] Xie J, Zhao C E, Lin Z Q, Gu P Y and Zhang Q C 2016 Nanostructured conjugated polymers for energy-related applications beyond solar cells Chem.—Asian J. 11 1489 Crossref

[134] Zhang G G, Lan Z A and Wang X C 2016 Conjugated polymers: catalysts for photocatalytic hydrogen evolution Angew. Chem., Int. Ed. Engl. 55 15712 Crossref

[135] Zhang J S, Zhang G G, Chen X F, Lin S, Mohlmann L, Dolega G, Lipner G, Antonietti M, Blechert S and Wang X C 2012 Co-monomer control of carbon nitride semiconductors to optimize hydrogen evolution with visible light Angew. Chem., Int. Ed. Engl. 51 3183 Crossref

[136] Chu S, Wang Y, Guo Y, Feng J Y, Wang C C, Luo W J, Fan X X and Zou Z G 2013 Band structure engineering of carbon nitride: in search of a polymer photocatalyst with high photooxidation property ACS Catal. 3 912 Crossref

[137] Sprick R S, Jiang J X, Bonillo B, Ren S J, Ratvijitvech T, Guiglion P, Zwijnenburg M A, Adams D J and Cooper A I 2015 Tunable organic photocatalysts for visible-light-driven hydrogen evolution J. Am. Chem. Soc. 137 3265 Crossref

[138] Vyas V S, Haase F, Stegbauer L, Savasci G, Podjaski F, Ochsenfeld C and Lotsch B V 2015 A tunable azine covalent organic framework platform for visible light-induced hydrogen generation Nat. Commun. 6 8508
Crossref

[139] You J B et al 2013 A polymer tandem solar cell with 10.6% power conversion efficiency Nat. Commun. 4 1446
Crossref

[140] Bourgeteau T, Tondelier D, Geffroy B, Brisse R, Cornut R, Artero V and Jousselme B 2015 Enhancing the performances of P3HT:PCBM-MoS3-based H2-evolving photocathodes with interfacial layers ACS Appl. Mater. Interfaces 7 16395 Crossref

[141] Rojas H C et al 2016 Polymer-based photocathodes with a solution-processable cuprous iodide anode layer and a polyethyleneimine protective coating Energy Environ. Sci. 9 3710 Crossref

[142] Fujishima A and Honda K 1972 Electrochemical photolysis of water at a semiconductor electrode Nature 238 37 Crossref

[143] Nozik A J 1975 Photoelectrolysis of water using semiconducting TiO2 crystals Nature 257 383
Crossref

[144] Watanabe T, Fujishima A and Honda K 1976 Photoelectrochemical reactions at SrTiO3 single-crystal electrode Bull. Chem. Soc. Japan 49 355 Crossref

[145] Wrighton M S, Ellis A B, Wolczanski P T, Morse D L, Abrahamson H B and Ginley D S 1976 Strontium-titanate photoelectrodes—efficient photoassisted electrolysis of water at zero applied potential J. Am. Chem. Soc. 98 2774 Crossref

[146] Li Z, Luo W, Zhang M, Feng J and Zou Z 2013 Photoelectrochemical cells for solar hydrogen production: current state of promising photoelectrodes, methods to improve their properties, and outlook Energy Environ. Sci. 6 347 Crossref

[147] Gan J, Lu X and Tong Y 2014 Towards highly efficient photoanodes: boosting sunlight-driven semiconductor nanomaterials for water oxidation Nanoscale 6 7142 Crossref

[148] Yang Y, Niu S, Han D, Liu T, Wang G and Li Y 2017 Progress in developing metal oxide nanomaterials for photoelectrochemical water splitting Adv. Energy Mater. 7 1700555 Crossref

[149] Jiang C, Moniz S J A, Wang A, Zhang T and Tang J 2017 Photoelectrochemical devices for solar water splitting—materials and challenges Chem. Soc. Rev. 46 4645 Crossref

[150] Sivula K, Le Formal F and Gratzel M 2011 Solar water splitting: progress using hematite (&agr;-Fe2O3) photoelectrodes ChemSusChem 4 432 Crossref

[151] Zandi O and Hamann T W 2016 Determination of photoelectrochemical water oxidation intermediates on haematite electrode surfaces using operando infrared spectroscopy Nat. Chem. 8 778
Crossref

[152] Li W, Sheehan S W, He D, He Y M, Yao X H, Grimm R L, Brudvig G W and Wang D W 2015 Hematite-based solar water splitting in acidic solutions: functionalization by mono- and multilayers of iridium oxygen-evolution catalysts Angew. Chem., Int. Ed. Engl. 54 11428
Crossref

[153] Kim J Y, Magesh G, Youn D H, Jang J W, Kubota J, Domen K and Lee J S 2013 Singlecrystalline, wormlike hematite photoanodes for efficient solar water splitting Sci. Rep. 3 2681
Crossref

[154] Shen S, Lindley S A, Chen X and Zhang J Z 2016 Hematite heterostructures for photoelectrochemical water splitting: rational materials design and charge carrier dynamics Energy Environ. Sci. 9 2744
Crossref

[155] Peerakiatkhajohn P, Yun J H, Chen H J, Lyu M Q, Butburee T and Wang L Z 2016 Stable hematite nanosheet photoanodes for enhanced photoelectrochemical water splitting Adv. Mater. 28 6405
Crossref

[156] Mayer M T 2017 Photovoltage at semiconductor–electrolyte junctions Curr. Opin. Electrochem. 2 104
Crossref

[157] Jang J-W et al 2015 Enabling unassisted solar water splitting by iron oxide and silicon Nat. Commun. 6 7447 Crossref

[158] Luo W J, Yang Z S, Li Z S, Zhang J Y, Liu J G, Zhao Z Y, Wang Z Q, Yan S C, Yu T and Zou Z G
2011 Solar hydrogen generation from seawater with a modified BiVO4 photoanode Energy Environ. Sci. 4 4046
Crossref

[159] Seabold J A and Choi K-S 2012 Efficient and stable photo-oxidation of water by a bismuth vanadate photoanode coupled with an iron oxyhydroxide oxygen evolution catalyst J. Am. Chem. Soc. 134 2186
Crossref

[160] McDonald K J and Choi K-S 2012 A new electrochemical synthesis route for a BiOI electrode and its conversion to a highly efficient porous BiVO4 photoanode for solar water oxidation Energy Environ. Sci. 5 8553
Crossref

[161] Abdi F F, Han L, Smets A H M, Zeman M, Dam B and van de Krol R 2013 Efficient solar water splitting by enhanced charge separation in a bismuth vanadate-silicon tandem photoelectrode Nat. Commun. 4 2195 Crossref

[162] Kim T W, Ping Y, Galli G A and Choi K S 2015 Simultaneous enhancements in photon absorption and charge transport of bismuth vanadate photoanodes for solar water splitting Nat. Commun. 6 8769
Crossref

[163] Wang Y, Li F, Zhou X, Yu F, Du J, Bai L and Sun L 2017 Highly efficient photoelectrochemical water splitting with an immobilized molecular Co4O4 cubane catalyst Angew. Chem. Int. Ed. Engl. 56 6911
Crossref

[164] Park Y, McDonald K J and Choi K-S 2013 Progress in bismuth vanadate photoanodes for use in solar water oxidation Chem. Soc. Rev. 42 2321 Crossref

[165] Rettie A J, Lee H C, Marshall L G, Lin J F, Capan C, Lindemuth J, McCloy J S, Zhou J, Bard A J and Mullins C B 2013 Combined charge carrier transport and photoelectrochemical characterization of BiVO4 single crystals: intrinsic behavior of a complex metal oxide J. Am. Chem. Soc. 135 11389
Crossref

[166] Abdi F F, Savenije T J, May M M, Dam B and van de Krol R 2013 The origin of slow carrier transport in BiVO4 thin film photoanodes: a time-resolved microwave conductivity study J. Phys. Chem. Lett. 4 2752
Crossref

[167] Kim T W and Choi K-S 2014 Nanoporous BiVO4 photoanodes with dual-layer oxygen evolution catalysts for solar water splitting Science 343 990 Crossref

[168] Qiu Y, Liu W, Chen W, Zhou G, Hsu P-C, Zhang R, Liang Z, Fan S, Zhang Y and Cui Y 2016 Efficient solar-driven water splitting by nanocone BiVO4-perovskite tandem cells Sci. Adv. 2 e1501764
Crossref

[169] Kuang Y, Jia Q, Nishiyama H, Yamada T, Kudo A and Domen K 2016 A front-illuminated nanostructured transparent BiVO4 photoanode for >2% efficient water splitting Adv. Energy Mater. 6 1501645
Crossref

[170] Mayer M T, Lin Y J, Yuan G B and Wang D W 2013 Forming heterojunctions at the nanoscale for improved photoelectrochemical water splitting by semiconductor materials: case studies on hematite Acc. Chem. Res. 46 1558 Crossref

[171] Yuan Y P, Ruan L W, Barber J, Loo S C J and Xue C 2014 Hetero-nanostructured suspended photocatalysts for solar-to-fuel conversion Energy Environ. Sci. 7 3934 Crossref

[172] Pihosh Y et al 2015 Photocatalytic generation of hydrogen by core–shell WO3/BiVO4 nanorods with ultimate water splitting efficiency Nat. Commun. 5 11141 Crossref

[173] Kim J H, Jang J-W, Jo Y H, Abdi F F, Lee Y H, van de Krol R and Lee J S 2016 Hetero-type dual photoanodes for unbiased solar water splitting with extended light harvesting Nat. Commun. 7 13380
Crossref

[174] Dillert R, Taffa D H, Wark M, Bredow T and Bahnemann D W 2015 Research update: photoelectrochemical water splitting and photocatalytic hydrogen production using ferrites (MFe2O4) under visible light irradiation APL Mater. 3 104001 Crossref

[175] Kim J H, Kim J H, Jang J W, Kim J Y, Choi S H, Magesh G, Lee J and Lee J S 2015 Awakening solar water-splitting activity of ZnFe2O4 nanorods by hybrid microwave annealing Adv.

Energy Mater. 5 1401933 Crossref

[176] Hufnagel A G, Peters K, Muller A, Scheu C, Ng D F R and Bein T 2016 Zinc ferrite photoanode nanomorphologies with favorable kinetics for water-splitting Adv. Funct. Mater. 26 4435
Crossref

[177] Guo Y S, Zhang N S, Wang X, Qian Q F, Zhang S Y, Li Z S and Zou Z G 2017 A facile spray pyrolysis method to prepare Ti-doped ZnFe2O4 for boosting photoelectrochemical water splitting J. Mater. Chem. A 5 7571 Crossref

[178] Guijarro N, Bornoz P, Prévot M S, Yu X, Johnson M, Le Formal F and Sivula K 2017 Spinel ferrites MFe2O4 (M = Cu, Mg, Zn) as emerging photoanodes for water oxidation: an in-depth analysis of the photoelectrochemical properties p 1523 MA2017-01

[179] Yourey J E and Bartlett B M 2011 Electrochemical deposition and photoelectrochemistry of CuWO4, a promising photoanode for water oxidation J. Mater. Chem. 21 7651 Crossref

[180] Chang Y C, Braun A, Deangelis A, Kaneshiro J and Gaillard N 2011 Effect of thermal treatment on the crystallographic, surface energetics, and photoelectrochemical properties of reactively cosputtered copper tungstate for water splitting J. Phys. Chem. C 115 25490 Crossref

[181] Pyper K J, Yourey J E and Bartlett B M 2013 Reactivity of CuWO4 in photoelectrochemical water oxidation is dictated by a midgap electronic state J. Phys. Chem. C 117 24726 Crossref

[182] Ye W, Chen F, Zhao F, Han N and Li Y 2016 CuWO4 nanoflake array-based single-junction and heterojunction photoanodes for photoelectrochemical water oxidation ACS Appl. Mater. Interfaces 8 9211
Crossref

[183] Gao Y, Zandi O and Hamann T W 2016 Atomic layer stack deposition-annealing synthesis of CuWO4 J. Mater. Chem. A 4 2826 Crossref

[184] Gao Y and Hamann T W 2017 Quantitative hole collection for photoelectrochemical water oxidation with CuWO4 Chem. Commun. 53 1285

[185] Biswas S K and Baeg J O 2013 Enhanced photoactivity of visible light responsive W incorporated FeVO4 photoanode for solar water splitting Int. J. Hydrog. Energy 38 14451
Crossref

Crossref

[186] Mandal H, Shyamal S, Hajra P, Bera A, Sariket D, Kundu S and Bhattacharya C 2016 Development of ternary iron vanadium oxide semiconductors for applications in photoelectrochemical water oxidation RSC Adv. 6 4992 Crossref

[187] Wang W, Zhang Y J, Wang L and Bi Y P 2017 Facile synthesis of Fe3+/Fe2+ self-doped nanoporous FeVO4 photoanodes for efficient solar water splitting J. Mater. Chem. A 5 2478 Crossref

[188] Quiñonero J and Gómez R 2017 Controlling the amount of co-catalyst as a critical factor in determining the efficiency of photoelectrodes: the case of nickel (II) hydroxide on vanadate photoanodes Appl. Catal. B 217 437 Crossref

[189] Maeda K and Domen K 2007 New non-oxide photocatalysts designed for overall water splitting under visible light J. Phys. Chem. C 111 7851 Crossref

[190] Liu G J, Shi J Y, Zhang F X, Chen Z, Han J F, Ding C M, Chen S S, Wang Z L, Han H X and Li C 2014 A tantalum nitride photoanode modified with a hole-storage layer for highly stable solar water splitting Angew. Chem. Int. Ed. Engl. 53 7295 Crossref

[191] Liu G J, Ye S, Yan P L, Xiong F Q, Fu P, Wang Z L, Chen Z, Shi J Y and Li C 2016 Enabling an integrated tantalum nitride photoanode to approach the theoretical photocurrent limit for solar water splitting Energy Environ. Sci. 9 1327 Crossref

[192] Liao M J, Feng J Y, Luo W J, Wang Z Q, Zhang J Y, Li Z S, Yu T and Zou Z G 2012 Co3O4 nanoparticles as robust water oxidation catalysts towards remarkably enhanced photostability of a Ta3N5 photoanode Adv. Funct. Mater. 22 3066 Crossref

[193] Li M X, Luo W J, Cao D P, Zhao X, Li Z S, Yu T and Zou Z G 2013 A co-catalyst-loaded Ta3N5 photoanode with a high solar photocurrent for water splitting upon facile removal of the surface layer Angew. Chem. Int. Ed. Engl. 52 11016

[194] Zhen C, Wang L Z, Liu G, Lu G Q and Cheng H M 2013 Template-free synthesis of Ta3N5 nanorod arrays for efficient photoelectrochemical water splitting Chem. Commun. 49 3019 Crossref

[195] Li Y B et al 2013 Cobalt phosphate-modified barium-doped tantalum nitride nanorod photoanode with 1.5% solar energy conversion efficiency Nat. Commun. 4 2566 Crossref

Crossref

[196] Wang L, Dionigi F, Nguyen N T, Kirchgeorg R, Gliech M, Grigorescu S, Strasser P and Schmuki P 2015 Tantalum nitride nanorod arrays: introducing Ni–Fe layered double hydroxides as a cocatalyst strongly stabilizing photoanodes in water splitting Chem. Mater. 27 2360 Crossref

[197] Zhong M et al 2017 Highly active GaN-stabilized Ta3N5 thin-film photoanode for solar water oxidation Angew. Chem. Int. Ed. Engl. 56 4739 Crossref

[198] Seo J, Takata T, Nakabayashi M, Hisatomi T, Shibata N, Minegishi T and Domen K 2015 Mg–Zr cosubstituted Ta3N5 photoanode for lower-onset-potential solar-driven photoelectrochemical water splitting J. Am. Chem. Soc. 137 12780 Crossref

[199] He Y, Thorne James E, Wu Cheng H, Ma P, Du C, Dong Q, Guo J and Wang D 2016 What limits the performance of Ta3N5 for solar water splitting? Chem 1 640 Crossref

[200] Nishimura N, Raphael B, Maeda K, Le Gendre L, Abe R, Kubota J and Domen K 2010 Effect of TiCl4 treatment on the photoelectrochemical properties of LaTiO2N electrodes for water splitting under visible light Thin Solid Films 518 5855 Crossref

[201] Leroy C M, Maegli A E, Sivula K, Hisatomi T, Xanthopoulos N, Otal E H, Yoon S, Weidenkaff A, Sanjines R and Gratzel M 2012 LaTiO2N/In2O3 photoanodes with improved performance for solar water splitting Chem. Commun. 48 820 Crossref

[202] Minegishi T, Nishimura N, Kubota J and Domen K 2013 Photoelectrochemical properties of LaTiO2N electrodes prepared by particle transfer for sunlight-driven water splitting Chem. Sci. 4 1120

Crossref

[203] Feng J Y, Luo W J, Fang T, Lv H, Wang Z Q, Gao J, Liu W M, Yu T, Li Z S and Zou Z G 2014 Highly photo-responsive LaTiO2N photoanodes by improvement of charge carrier transport among film particles Adv. Funct. Mater. 24 3535 Crossref

[204] Akiyama S et al 2016 Highly efficient water oxidation photoanode made of surface modified LaTiO2N particles Small 12 5468 Crossref

[205] Higashi M, Domen K and Abe R 2013 Fabrication of an efficient BaTaO2N photoanode harvesting a wide range of visible light for water splitting J. Am. Chem. Soc. 135 10238 Crossref

[206] Ueda K et al 2015 Photoelectrochemical oxidation of water using BaTaO2N photoanodes prepared by particle transfer method J. Am. Chem. Soc. 137 2227 Crossref

[207] Kodera M, Urabe H, Katayama M, Hisatomi T, Minegishi T and Domen K 2016 Effects of flux synthesis on SrNbO2N particles for photoelectrochemical water splitting J. Mater. Chem. A 4 7658
Crossref

[208] Hajibabaei H, Zandi O and Hamann T W 2016 Tantalum nitride films integrated with transparent conductive oxide substrates via atomic layer deposition for photoelectrochemical water splitting Chem. Sci. 7 6760 Crossref

[209] Fujii K and Ohkawa K 2006 Hydrogen generation from aqueous water using n-GaN by photoassisted electrolysis Phys. Status Solidi c 3 2270 Crossref

[210] Luo W J, Liu B, Li Z S, Xie Z L, Chen D J, Zou Z G and Zhang R 2008 Stable response to visible light of InGaN photoelectrodes Appl. Phys. Lett. 92 262110 Crossref

[211] Li J, Lin J Y and Jiang H X 2008 Direct hydrogen gas generation by using InGaN epilayers as working electrodes Appl. Phys. Lett. 93 162107 Crossref

[212] Li M X, Luo W J, Liu B, Zhao X, Li Z S, Chen D J, Yu T, Xie Z L, Zhang R and Zou Z G 2011 Remarkable enhancement in photocurrent of In0.20Ga0.80N photoanode by using an electrochemical surface treatment Appl. Phys. Lett. 99 112108 Crossref

[213] Caccamo L et al 2014 Band engineered epitaxial 3D GaN-InGaN core–shell rod arrays as an advanced photoanode for visible-light-driven water splitting ACS Appl. Mater. Interfaces 6 2235
Crossref

[214] Ebaid M, Kang J H, Lim S H, Ha J S, Lee J K, Cho Y H and Ryu S W 2015 Enhanced solar hydrogen generation of high density, high aspect ratio, coaxial InGaN/GaN multi-quantum well nanowires Nano Energy 12 215 Crossref

[215] Fan S, Woo S Y, Vanka S, Botton G A and Mi Z 2016 An In0.5Ga0.5N nanowire photoanode for harvesting deep visible light photons APL Mater. 4 076106 Crossref

[216] AlOtaibi B, Nguyen H P T, Zhao S, Kibria M G, Fan S and Mi Z 2013 Highly stable photoelectrochemical water splitting and hydrogen generation using a double-band InGaN/GaN core/shell nanowire photoanode Nano Lett. 13 4356 Crossref

[217] Fan S, Shih I and Mi Z 2017 A monolithically integrated InGaN nanowire/Si tandem photoanode approaching the ideal bandgap configuration of 1.75/1.13 eV Adv. Energy Mater. 7 1600952
Crossref

[218] Mei B, Seger B, Pedersen T, Malizia M, Hansen O, Chorkendorff I and Vesborg P C K 2014 Protection of p+–n–Si photoanodes by sputter-deposited Ir/IrOx thin films J. Phys. Chem. Lett. 5 1948
Crossref

[219] Zhou X, Liu R, Sun K, Papadantonakis K M, Brunschwig B S and Lewis N S 2016 570 mV photovoltage, stabilized n-Si/CoOx heterojunction photoanodes fabricated using atomic layer deposition Energy Environ. Sci. 9 892 Crossref

[220] Yang J et al 2017 A multifunctional biphasic water splitting catalyst tailored for integration with high-performance semiconductor photoanodes Nat. Mater. 16 335 Crossref

[221] Yu X, Yang P, Chen S, Zhang M and Shi G 2017 NiFe alloy protected silicon photoanode for efficient water splitting Adv. Energy Mater. 7 1601805 Crossref

[222] Kainthla R C, Zelenay B and Bockris J O M 1986 Protection of n-Si photoanode against photocorrosion in photoelectrochemical cell for water electrolysis J. Electrochem. Soc. 133 248
Crossref

[223] Li G and Wang S 1987 Photoelectrochemical characteristics of metal-modified epitaxial n-Si anodes J. Electroanal. Chem. Interfacial Electrochem. 227 213 Crossref

[224] Sun K et al 2012 Nickel oxide functionalized silicon for efficient photo-oxidation of water Energy Environ. Sci. 5 7872 Crossref

[225] Jun K, Lee Y S, Buonassisi T and Jacobson J M 2012 High photocurrent in silicon photoanodes catalyzed by iron oxide thin films for water oxidation Angew. Chem. Int. Ed. Engl. 51 423 Crossref

[226] Sun K, Pang X, Shen S, Qian X, Cheung J S and Wang D 2013 Metal oxide composite enabled nanotextured si photoanode for efficient solar driven water oxidation Nano Lett. 13 2064
Crossref

[227] Strandwitz N C, Comstock D J, Grimm R L, Nichols-Nielander A C, Elam J and Lewis N S 2013 Photoelectrochemical behavior of n-type Si(100) electrodes coated with thin films of manganese oxide grown by atomic layer deposition J. Phys. Chem. C 117 4931 Crossref

[228] Chen Y W, Prange J D, Dühnen S, Park Y, Gunji M, Chidsey C E D and McIntyre P C 2011 Atomic layer-deposited tunnel oxide stabilizes silicon photoanodes for water oxidation Nat. Mater. 10 539
Crossref

[229] Kenney M J, Gong M, Li Y, Wu J Z, Feng J, Lanza M and Dai H 2013 High-performance silicon photoanodes passivated with ultrathin nickel films for water oxidation Science 342 836 Crossref

[230] Hu S, Shaner M R, Beardslee J A, Lichterman M, Brunschwig B S and Lewis N S 2014 Amorphous TiO2 coatings stabilize Si, GaAs, and GaP photoanodes for efficient water oxidation Science 344 1005 Crossref

[231] Hu S, Richter M H, Lichterman M F, Beardslee J, Mayer T, Brunschwig B S and Lewis N S 2016 Electrical, photoelectrochemical, and photoelectron spectroscopic investigation of the interfacial transport and energetics of amorphous TiO2/Si heterojunctions J. Phys. Chem. C 120 3117
Crossref

[232] Chen L et al 2015 p-type transparent conducting oxide/n-type semiconductor heterojunctions for efficient and stable solar water oxidation J. Am. Chem. Soc. 137 9595 Crossref

[233] Sun K, Kuang Y J, Verlage E, Brunschwig B S, Tu C W and Lewis N S 2015 Sputtered NiOx films for stabilization of p+n-InP photoanodes for solar-driven water oxidation Adv. Energy Mater. 5 1402276
Crossref

[234] Verlage E, Hu S, Liu R, Jones R J R, Sun K, Xiang C X, Lewis N S and Atwater H A 2015 A monolithically integrated, intrinsically safe, 10% efficient, solar-driven water-splitting system based on active, stable earth-abundant electrocatalysts in conjunction with tandem III–V light absorbers protected by amorphous TiO2 films Energy Environ. Sci. 8 3166 Crossref

[235] Wang X C, Maeda K, Thomas A, Takanabe K, Xin G, Carlsson J M, Domen K and Antonietti M 2009 A metal-free polymeric photocatalyst for hydrogen production from water under visible light Nat. Mater. 8 76 Crossref

[236] Wang X C, Maeda K, Chen X F, Takanabe K, Domen K, Hou Y D, Fu X Z and Antonietti M 2009 Polymer semiconductors for artificial photosynthesis: hydrogen evolution by mesoporous graphitic carbon nitride with visible light J. Am. Chem. Soc. 131 1680 Crossref

[237] Zhang Y J and Antonietti M 2010 Photocurrent generation by polymeric carbon nitride solids: an initial step towards a novel photovoltaic system Chem.—Asian J. 5 1307 Crossref

[238] Chu S, Wang C C, Feng J Y, Wang Y and Zou Z G 2014 Melem: a metal-free unit for photocatalytic hydrogen evolution Int. J. Hydrog. Energy 39 13519

Crossref

[239] Bian J C, Xi L F, Huang C, Lange K M, Zhang R Q and Shalom M 2016 Efficiency enhancement of carbon nitride photoelectrochemical cells via tailored monomers design Adv. Energy Mater. 6 1600263 Crossref

[240] Ruan Q, Luo W, Xie J, Wang Y, Liu X, Bai Z, Carmalt C J and Tang J 2017 A nanojunction polymer photoelectrode for efficient charge transport and separation Angew. Chem. Int. Ed. Engl. 56 8221
Crossref

[241] Bornoz P, Prevot M S, Yu X Y, Guijarro N and Sivula K 2015 Direct light-driven water oxidation by a ladder-type conjugated polymer photoanode J. Am. Chem. Soc. 137 15338 Crossref

[242] King L A, Zhao W, Chhowalla M, Riley D J and Eda G 2013 Photoelectrochemical properties of chemically exfoliated MoS2 J. Mater. Chem. A 1 8935 Crossref

[243] Yin Z, Chen B, Bosman M, Cao X, Chen J, Zheng B and Zhang H 2014 Au nanoparticlemodified MoS2 nanosheet-based photoelectrochemical cells for water splitting Small 10
3537

Crossref

[244] Xu X, Zhou G, Dong X and Hu J 2017 Interface band engineering charge transfer for 3D MoS2 photoanode to boost photoelectrochemical water splitting ACS Sustain. Chem. Eng. 5 3829
Crossref

[245] Jacobsson T J, Fjallstrom V, Edoff M and Edvinsson T 2015 A theoretical analysis of optical absorption limits and performance of tandem devices and series interconnected architectures for solar hydrogen production Sol. Energy Mater. Sol. Cells 138 86 Crossref

[246] Yoneyama H, Sakamoto H and Tamura H 1975 Photo-electrochemical cell with production of hydrogen and oxygen by a cell reaction Electrochim. Acta 20 341 Crossref

[247] Nozik A J 1976 p–n photoelectrolysis cells Appl. Phys. Lett. 29 150 Crossref

[248] Ohashi K, Mccann J and Bockris J O M 1977 Stable photoelectrochemical cells for splitting of water Nature 266 610 Crossref

[249] Mor G K, Varghese O K, Wilke R H T, Sharma S, Shankar K, Latempa T J, Choi K S and Grimes C A 2008 p-type Cu–Ti–O nanotube arrays and their use in self-biased heterojunction photoelectrochemical diodes for hydrogen generation Nano Lett. 8 1906 Crossref

[250] Liu C, Tang J Y, Chen H M, Liu B and Yang P D 2013 A fully integrated nanosystem of semiconductor nanowires for direct solar water splitting Nano Lett. 13 2989 Crossref

[251] Kargar A, Khamwannah J, Liu C H, Park N, Wang D, Dayeh S A and Jin S H 2016 Nanowire/nanotube array tandem cells for overall solar neutral water splitting Nano Energy 19 289
Crossref

[252] Shaner M R, McDowell M T, Pien A, Atwater H A and Lewis N S 2016 Si/TiO2 tandemjunction microwire arrays for unassisted solar-driven water splitting J. Electrochem. Soc.
163 H261
Crossref

[253] Wang H L, Deutsch T and Turner J A 2008 Direct water splitting under visible light with nanostructured hematite and WO3 photoanodes and a GaInP2 photocathode J. Electrochem. Soc. 155 F91 Crossref

[254] Chen Q P, Li J H, Li X J, Huang K, Zhou B X and Shangguan W F 2013 Self-biasing photoelectrochemical cell for spontaneous overall water splitting under visible-light illumination ChemSusChem 6 1276 Crossref

[255] Walczak K et al 2015 Modeling, simulation, and fabrication of a fully integrated, acid-stable, scalable solar-driven water-splitting system ChemSusChem 8 544 Crossref

[256] Bornoz P, Abdi F F, Tilley S D, Dam B, van de Krol R, Graetzel M and Sivula K 2014 A Bismuth vanadate-cuprous oxide tandem cell for overall solar water splitting J. Phys. Chem. C 118 16959
Crossref

[257] Kornienko N, Gibson N A, Zhang H, Eaton S W, Yu Y, Aloni S, Leone S R and Yang P D 2016 Growth and photoelectrochemical energy conversion of wurtzite indium phosphide nanowire arrays ACS Nano 10 5525 Crossref

[258] Kato T, Hakari Y, Ikeda S, Jia Q X, Iwase A and Kudo A 2015 Utilization of metal sulfide material of (CuGa)1−xZn2xS2 solid solution with visible light response in photocatalytic and photoelectrochemical solar water splitting systems J. Phys. Chem. Lett. 6 1042 Crossref

[259] Kim J H, Kaneko H, Minegishi T, Kubota J, Domen K and Lee J S 2016 Overall photoelectrochemical water splitting using tandem cell under simulated sunlight ChemSusChem 9 61
Crossref

[260] Lai Y H, Palm D W and Reisner E 2015 Multifunctional coatings from scalable single source precursor chemistry in tandem photoelectrochemical water splitting Adv. Energy Mater. 5 1501668
Crossref

[261] Xu P, Feng J Y, Fang T, Zhao X, Li Z S and Zou Z G 2016 Photoelectrochemical cell for unassisted overall solar water splitting using a BiVO4 photoanode and Si nanoarray photocathode RSC Adv. 6 9905 Crossref

[262] Cooper J K, Gul S, Toma F M, Chen L, Liu Y S, Guo J H, Ager J W, Yano J and Sharp I D 2015 Indirect bandgap and optical properties of monoclinic bismuth vanadate J. Phys. Chem. C 119 2969
Crossref

[263] Ye K H, Wang Z, Gu J, Xiang S, Yuan Y, Zhu Y, Zhang Y, Mai W and Yang S 2017 Carbon quantum dots as a visible light sensitizer to significantly increase the solar water splitting performance of bismuth vanadate photoanodes Energy Environ. Sci. 10 772 Crossref

[264] Tolod K, Hernández S and Russo N 2017 Recent advances in the BiVO4 photocatalyst for sun-driven water oxidation: top-performing photoanodes and scale-up challenges Catalysts 7 13 Crossref

[265] Jin J, Walczak K, Singh M R, Karp C, Lewis N S and Xiang C X 2014 An experimental and modeling/simulation-based evaluation of the efficiency and operational performance characteristics of an integrated, membrane-free, neutral pH solar-driven water-splitting system Energy Environ. Sci. 7 3371 Crossref

[266] Singh M R, Papadantonakis K, Xiang C X and Lewis N S 2015 An electrochemical engineering assessment of the operational conditions and constraints for solar-driven water-splitting systems at near-neutral pH Energy Environ. Sci. 8 2760 Crossref

[267] Yang H B, Miao J W, Hung S F, Huo F W, Chen H M and Liu B 2014 Stable quantum dot photoelectrolysis cell for unassisted visible light solar water splitting ACS Nano 8 10403 Crossref

[268] Bai Z M and Zhang Y H 2017 A Cu2O/Cu2S–ZnO/CdS tandem photoelectrochemical cell for self-driven solar water splitting J. Alloys Compd. 698 133 Crossref

[269] AlOtaibi B, Fan S, Vanka S, Kibria M G and Mi Z 2015 A metal-nitride nanowire dualphotoelectrode device for unassisted solar-to-hydrogen conversion under parallel illumination Nano Lett. 15 6821 Crossref

[270] Kment S, Riboni F, Pausova S, Wang L, Wang L, Han H, Hubicka Z, Krysa J, Schmuki P and Zboril R 2017 Photoanodes based on TiO2 and &agr;-Fe2O3 for solar water splitting— superior role of 1D nanoarchitectures and of combined heterostructures Chem. Soc. Rev. 46 3716 Crossref

[271] Sharp I D, Cooper J K, Toma F M and Buonsanti R 2017 Bismuth vanadate as a platform for accelerating discovery and development of complex transition-metal oxide photoanodes ACS Energy Lett. 2 139
Crossref

[272] Bae D, Seger B, Vesborg P C K, Hansen O and Chorkendorff I 2017 Strategies for stable water splitting via protected photoelectrodes Chem. Soc. Rev. 46 1933 Crossref

[273] Hu S, Lewis N S, Ager J W, Yang J H, McKone J R and Strandwitz N C 2015 Thin-film materials for the protection of semiconducting photoelectrodes in solar-fuel generators J. Phys. Chem. C 119 24201 Crossref

[274] Scheuermann A G and McIntyre P C 2016 Atomic layer deposited corrosion protection: a path to stable and efficient photoelectrochemical cells J. Phys. Chem. Lett. 7 2867 Crossref

[275] Shaner M R, Hu S, Sun K and Lewis N S 2015 Stabilization of Si microwire arrays for solardriven H2O oxidation to O2(g) in 1.0 M KOH(aq) using conformal coatings of amorphous TiO2 Energy Environ. Sci. 8 203 Crossref

[276] Crespo-Quesada M and Reisner E 2017 Emerging approaches to stabilise photocorrodible electrodes and catalysts for solar fuel applications Energy Environ. Sci. 10 1116 Crossref

[277] Abdi F F and Berglund S P 2017 Recent developments in complex metal oxide photoelectrodes J. Phys. D: Appl. Phys. 50 193002
IOPscience (http://iopscience.iop.org/0022-3727/50/19/193002)

[278] Cheng W H, Richter M H, May M M, Ohlmann J, Lackner D, Dimroth F, Hannappel T, Atwater H A and Lewerenz H J 2017 Monolithic photoelectrochemical device for 19% direct water splitting arXiv:1706.01493 [cond-mat.mtrl-sci] Preprint

Export references: BibTeX RIS

Citations

1. Photoelectrode for water splitting: Materials, fabrication and characterization
   Zhiliang Wang and Lianzhou Wang 2018 Science China Materials Crossref

2. Progress in designing effective photoelectrodes for solar water splitting
   Zhiliang Wang and Lianzhou Wang 2018 Chinese Journal of Catalysis 39 369 Crossref

3. Solar Water Oxidation by an InGaN Nanowire Photoanode with a Bandgap of 1.7 eV Sheng Chu et al 2018 ACS Energy Letters 3 307 Crossref

4. A review on photocatalytic CO_2 reduction using perovskite oxide nanomaterials
   Sheng Zeng et al 2018 Nanotechnology 29 052001
   IOPscience (/0957-4484/29/5/052001)

5. Co2 P Nanorods as an Efficient Cocatalyst Decorated Porous g-C3 N4 Nanosheets for Photocatalytic Hydrogen Production under Visible Light Irradiation

Deqian Zeng et al 2017 Particle & Particle Systems Characterization 1700251 Crossref

Related content

JOURNAL ARTICLES

Recent developments in complex metal oxide photoelectrodes

Surface- and interface-engineered heterostructures for solar hydrogen generation

Silicon nanowire heterostructures for advanced energy and environmental applications: a review

Controlled synthesis of GaN-based nanowires for photoelectrochemical water splitting applications

InP nanopore arrays for photoelectrochemical hydrogen generation

Improved charge separation efficiency of hematite photoanodes by coating an ultrathin p-type $LaFeO_3$ overlayer